Functionally Graded Adhesive Patch Repairs in Civil Applications

Guilherme Miranda Silva de Oliveira Viana

Master Thesis Report

Supervisor: Prof. Lucas F. M. da Silva

Co-Supervisor: Eng. Ricardo Carbas

Faculdade de Engenharia da Universidade do Porto

Mestrado Integrado em Engenharia Mecânica

June 2013

Abstract

Several investigations have been made concerning the fracture behaviour of scaled specimens of wood beams repaired with adhesively bonded carbon fibre reinforced plastic. However, one of the problems associated to these joints is the fact that the stress distribution (shear and peel) is concentrated at the ends of the overlap, leading to premature failure of the joint. Some solutions to this problem have been developed, such as hybrid joints, adherend shaping, adherend rounding and fillets at the ends of the overlap. Some of these methods tend to increase the weight of the structure and others are very expensive due to its complex manufacturing process.

The stress concentration can be reduced with use of a functionally graded adhesive, in which, the mechanical properties vary along the bondlength. This can be achieved with a graded cure, in which the temperature varies along the bondlength. In order to perform a graded cure, induction heating was used. This technique has already been successfully tested in single lap joints to obtain a more uniform stress distribution along the bondlength, increasing the strength of the joint. In this project, the repair of wood structures with CFRP was made using a homogeneous cure and a graded cure.

Two common types of defects on beams under bending solicitations were analysed. Scaled specimens of damaged wood beams were repaired and tested under four point bending. The results show that the beams repaired with a graded bondline were able to withstand higher loads.

Reparação de Estruturas Usando Ligações Adesivas Graduadas

Resumo

Têm sido feitas várias investigações sobre o comportamento mecânico de vigas de madeira à escala, reparadas com compósitos de fibra de carbono. Contudo é sabido que um dos problemas associados às ligações adesivas se prende com a concentração de tensões tanto no adesivo como nos substratos (no que concerne à tensão de corte e tensão de arrancamento) e pode levar à rotura prematura da junta. Várias soluções têm sido desenvolvidas para minimizar este problema, tal como o método dos dois adesivos, arredondamento das arestas dos substractos, utilização de filets, etc. Alguns destes métodos tendem a aumentar o peso da estrutura ou são demasiado dispendiosos devido à complexidade do processo de fabrico.

O problema da concentração de tensão pode ser minimizado com recurso a um adesivo graduado, em que as propriedades mecânicas variam ao longo do comprimento de sobreposição. Isto pode ser conseguido com uma cura graduada, em que a temperatura de cura varia com o comprimento de sobreposição. Para a obtenção de uma cura graduada, o adesivo é aquecido por indução nas zonas de maior concentração de tensão, ficando, nessas áreas, com uma maior flexibilidade e ductilidade. Esta técnica já foi testada com sucesso em juntas de sobreposição simples e foi utilizada novamente na reparação de vigas em madeira com fibra de carbono. Os resultados da reparação da viga com junta graduada são comparados com os da viga com cura isotérmica.

Foram analisados dois tipos de defeito comuns em vigas de madeira solicitadas à flexão. Foram fabricadas vigas de madeira à escala que tentam reproduzir esses mesmos defeitos. Esses provetes foram testados em flexão em quatro pontos. Os resultados mostram que as vigas reparadas com o adesivo graduado são capazes de aguentar cargas mais elevadas que as vigas reparadas com o adesivo homogéneo.

Acknowledgements

I would like to express my gratitude towards my supervisor Lucas F. M. da Silva and co-supervisor Ricardo Carbas for their guidance, technical contribution, dedication and writing review during this work.

I equally wish to thank engineers Eduardo Marques and Raul Campilho for their help with the finite element software Abaqus®. Thanks to engineer Filipe Chaves for his help with the DCB and ENF tests.

Acknowledgements to my family and all my friends for their fellowship and encouraging support.

Finally I would like to express my sincere gratitude towards Sara Duque, who has supported me through all stages of this work.

Table of Contents

List of Tables

List of Figures

Nomenclature

Acronyms

CBBM	Compliance Based Beam Method
CFRP	Carbon Fibre Reinforced Plastic
CZM	Cohesive Zone Model
DCB	Double Cantilever Beam
ENF	End Notched Flexure
FEM	Finite Element Method
FEUP	Faculdade de Engenharia da Universidade do Porto
FPZ	Fracture Process Zone
FRP	Fibre Reinforced Plastic
GFRP	Glass Fibre Reinforced Plastic
2D	Two dimensions

Symbols

E	Young's Modulus
G	Shear Modulus
P	Load
v	Poisson's ratio
δ	Displacement
G_{IC}	Mode I fracture toughness
G_{IIC}	Mode II fracture toughness
τ	Shear stress
τ_{avg}	Average shear stress
σ	Peel stress

1 Introduction

1.1 Backgroung and Motivation

Wood is one of the most ancient building materials, however, nowadays, in Portugal, its use in civil structures is not a common practise. Other countries, such as the United States of America, Russia, Norway, Sweden, Finland, due to the many advantages that it presents, extensively use wood in civil construction. Figures 1-5 show different examples of wood constructions.

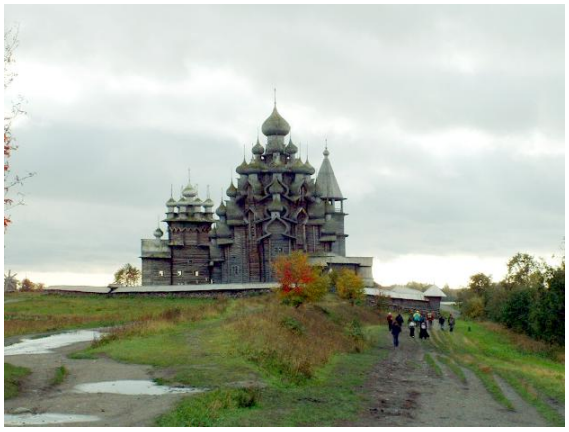

Figure 1: Church in Kizhi, Russia.

Figure 2: Leonardo Bridge, Aas, Norway.

Figure 3: Houses, Alborg, Denmark.

Figure 4: Stadium, Vantaa, Finland.

Figure 5: Pavilhão Atlântico, Portugal.

Wood is an inexpensive building material that can provide easy to build structures. Its thermal conductivity is low, providing good thermal isolation. It is also a good acoustic isolator. It has good specific mechanical properties (divided by its weight). However, if not properly preserved, it is easily degraded by atmospheric and biological agents, such as fungus and insects (1). It is also susceptible to moisture changes and fatigue for low stress differential (2).

Little pollution is created during wood production. It is a renewable and recyclable product.

Replacements of large timber sections are very expensive due to the complexity of the process and the limited availability of the material. When possible, timber beams should be repaired rather than replaced.

Timber structures repairs using structural adhesives are both economically and structurally efficient. Among the several types of adhesives, epoxy adhesives are the best for this kind of joint as they do not require high pressure during application, they exhibit good adhesion to wood and several other materials (such as FRP), little shrinkage during cure and are highly resistant to moisture and chemical products (3).

Several authors have witnessed the considerable improvement of the strength and stiffness of timber beams repaired with bonded FRP patches (4) (5) (6) (7) (8). However, one of the problems associated with this kind of joint is the stress concentration in both the adherends and the adhesive, which causes the premature failure of the joint (9) (4). In order to reduce this problem, several techniques have been developed, such as hybrid joints, adherend shaping, adherend rounding and fillets at the ends of the overlap, graded. These techniques are usually very expensive to implement due to the excessive steps in the manufacture process and tend to increase the weight of the structure.

It is known that graded adhesives can provide a significant improvement in the strength of adhesive joints (10). Many epoxy adhesives have different properties depending on their temperature of cure (11). If the temperature of cure may vary along the overlap, a gradient in the rigidity of the adhesive can be obtained. This can be used to make a functionally graded adhesive joint.

1.2 Objectives

The main objective of this research was to investigate the performance of a functionally graded adhesive in the repair of scaled damaged wood beams.

The specific objectives are listed below:

- Determine the cohesive laws of the adhesive (mode I and II) for three different temperatures of cure. This can be made using DCB and ENF specimens. The energy release rate can be computed using the CBBM method (12) (13), a recently developed technique that does not require the measurement of the crack length during propagation;
- Simulate the mechanical behaviour of the repaired beams using the FEM. CZM can be used in order to simulate crack propagation in both the adhesive and the wood;
- Conduct bending tests on damaged and undamaged beams, beams repaired with the functionally graded bondline and the beams repaired with an adhesive with constant properties.

1.3 Research Methodology

In order to achieve the objectives of this investigation, the following method was used:

- A literature review on the repair of wood beams, methods to increase the strength of adhesive joints and on strength prediction was made;
- DCB and ENF tests were made in order to assess the fracture toughness of the adhesive for three different temperatures of cure;
- The beams repaired with the functionally graded bondline and the beams repaired with an adhesive with constant properties were tested under four point bending. The results were compared;
- The repaired beams were numerically simulated using the FEM and CZM.

1.4 Outline of the Thesis

This thesis is divided into five chapters:

- **Chapter 1** is an introduction to the proceedings used and the format of the thesis;
- In **Chapter 2**, a review on the state of the art is made. It focus on the repair of wood beams, methods to increase the strength of adhesive joints and methods for strength prediction;
- In **Chapter 3**, the experimental work concerning the determination of the energy release rate of the adhesive in modes I and II is presented;
- **Chapter 4** focuses on the manufacture, test and numerical simulation of the wood beams;
- In **Chapter 5** the final observations and references to possible future investigations are made.

2 State-of-the-Art Review

2.1 Wood Structures

2.1.1 Common Defects in Wood Structures

Natural defects in wood include mainly knots, rots, wanes, shakes, checks and splits (Figure 6) (14).

Knots act as discontinuities in the wood, raising the stress concentration factor around it. In a beam under bending, knots should be placed in the compression face rather than in the tension face, as its contribution to reducing the strength of the beam is lower (1).

A wane is lack of wood on the edge or corner of wood members and shakes are lengthwise separations in the wood occurring between annual rings (1).

Checks and splits are cracks that occur along the direction of the tree's growth and are caused by shrinkages and swellings due to changes in the moisture of the wood (15) (1). This kind of crack acts severely as stress concentration points especially if the beam is under bending. Heart checks (checks that extend deep into the interior of the wood) expose the inner part of the wood member to fungus and insects, causing rots and lowering strength (16).

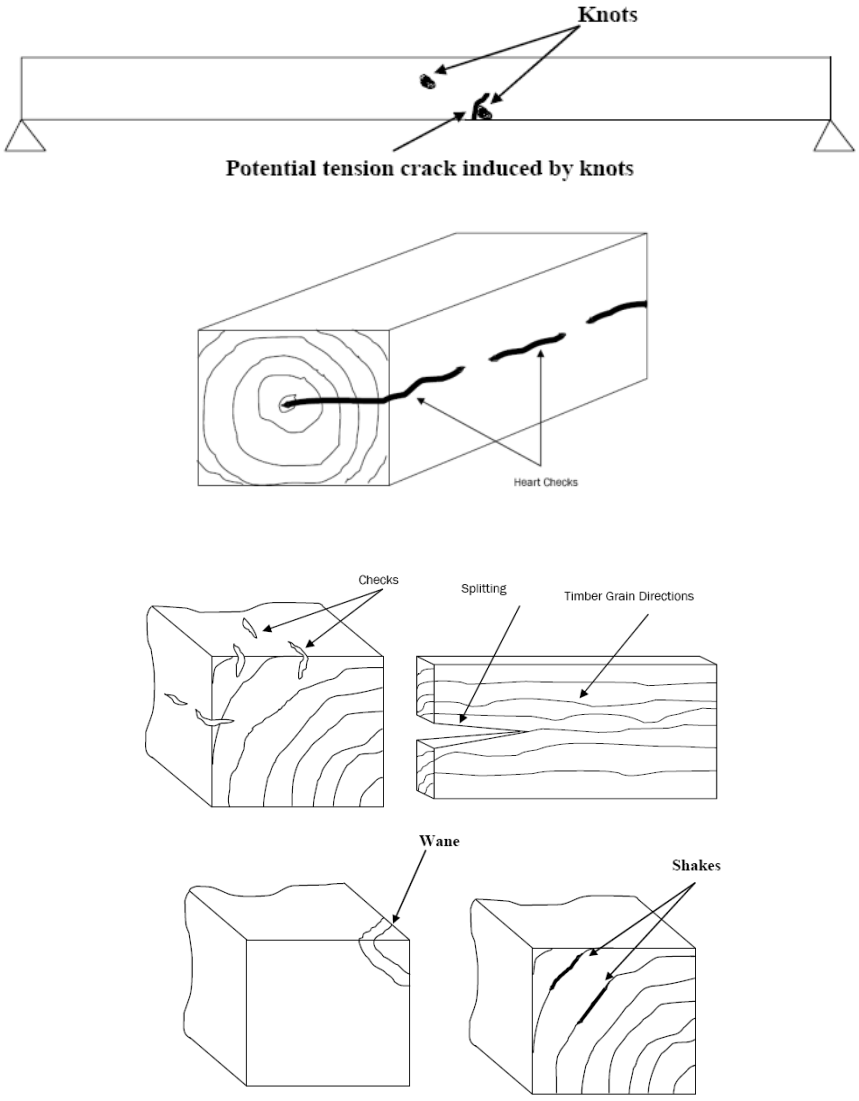

Figure 6: Natural defects in wood members **(1)**.

In-service damage of wood includes mainly compression failure, cross-grain tension and shear failure (1).

Compression failure is typical of low density wood or beams reinforced in the tension face, as the change of the neutral axis provides a larger cross section to bear the compressive load (1).

Cross-grain tension is common in beams whose fibres are not aligned with the main axis (Figure 7). This happens when the tree that is cut for lumber grows spirally or with a pronounced taper. The crack that is originated has usually an angle with the beam's axis of less than 15 degrees (1).

Horizontal shear cracks normally propagate from checks and shakes (Figure 8). If the beam is under extreme low humidity or shows sharp changes in growth ring density, this kind of failure is more likely to occur (1).

Tension failure can also occur if there is a knot in the tension face of the beam, as it acts as a point of stress concentration (5).

Figure 7: A cross grain tension crack **(1)**.

Figure 8: A horizontal shear crack **(1)**.

2.1.2 Repair of Wood Structures

Radford *et al*. (17) studied the effect of nails, shear glass fibre rods and plates in the repair of wood beams. Holes were drilled in the wood beam and shear spikes impregnated in epoxy adhesive were inserted, reinforcing the beam in shear. The adhesive was used to improve the load transfer from the wood to the spike, exclude the water from the interface, due to its compatibility with the materials and also to spread into the gaps the beam might have. As the spikes are inside the wood, the aesthetics are only marginally affected and no preservatives can possibly affect the quality of the joint.

In order to test the performance of the repaired beams, scale specimens were tested under three point bending. Glass fibre reinforced composite rods and steel nails were used as shear spikes. The beam's strength and stiffness was investigated for six repair configurations, as shown in Figure 9.

It was concluded that repairing with shear spikes impregnated in epoxy adhesive can recapture the undamaged strength and stiffness of the beam. The best results were achieved with glass fibre reinforced composite rods. Repair with bonded GFRP plates was also performed, although not being as effective as the shear spikes.

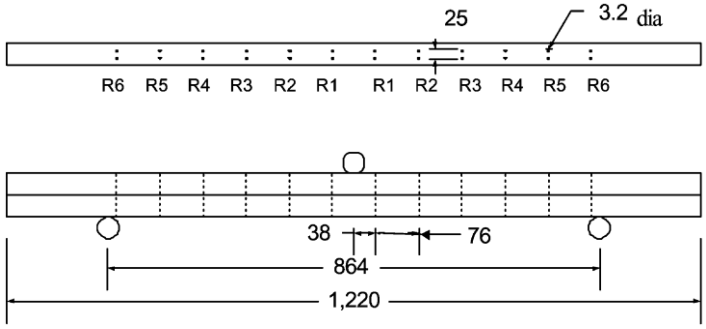

Figure 9: Schematic representation of the beams tested by Radford *et al* **(17)**.

Akbiyik (1) (14) focused on the repair of beams with horizontal splits from an old bridge in Texas. The repair techniques included the use of hex bolts, lag screws, FRP and plywood in the configurations seen in Figure 10.

All repaired beams were tested under four point bending and their ultimate load was measured and compared.

The best results were obtained for the beams repaired with GFRP as it improved both the strength and the stiffness of the beam. Using more hex bolts than the ideal has repercussions in the mechanical characteristics of the beam. The methods involving lag screws and plywood plates, though being effective repair methods, did not improve greatly the mechanical characteristics of the beam. Almost all repaired beams exhibited an increase in stiffness relatively to the beam without splits.

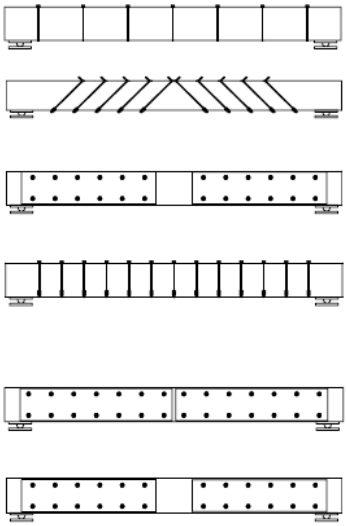

Figure 10: Schematic representation of the beams repaired by Akbiyik **(1) (14)**.

The work of Alam *et al.* (5) addressed the repair of spruce beams previously damaged in the laboratory under four point bending. The beams were loaded until the first drop in load occurred and were then flattened and repaired. As shown in Figure 11, several modes of failure were observed.

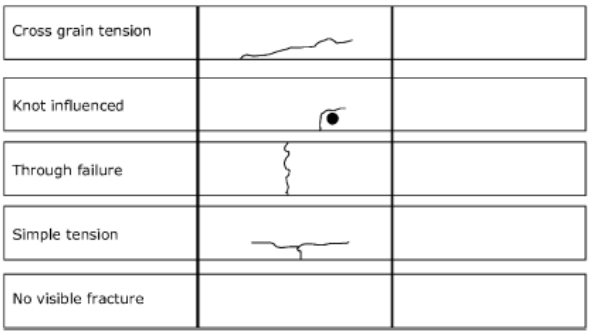

Figure 11: Types of failure in wood beams witnessed by Alam *et al* **(5)**.

The repairs were made using four rectangular section materials: mild steel, pultruded CFRP, pultruded glass fibre reinforced plastic and pultruded glass fibre reinforced thermoplastic polyurethane. Some of the beams were repaired only on the compression face, some were repaired on the tensile face and the remaining were repaired on both the compression and tensile face. The tests showed that repairing in both the tensile and compression face were more effective than repairing only in one face. Steel and CFRP have the greatest ability to enhance the flexural strength of the repaired beam. Figure 12 shows, for the two face repair and different materials analysed, the increase in flexural strength relatively to the undamaged beam.

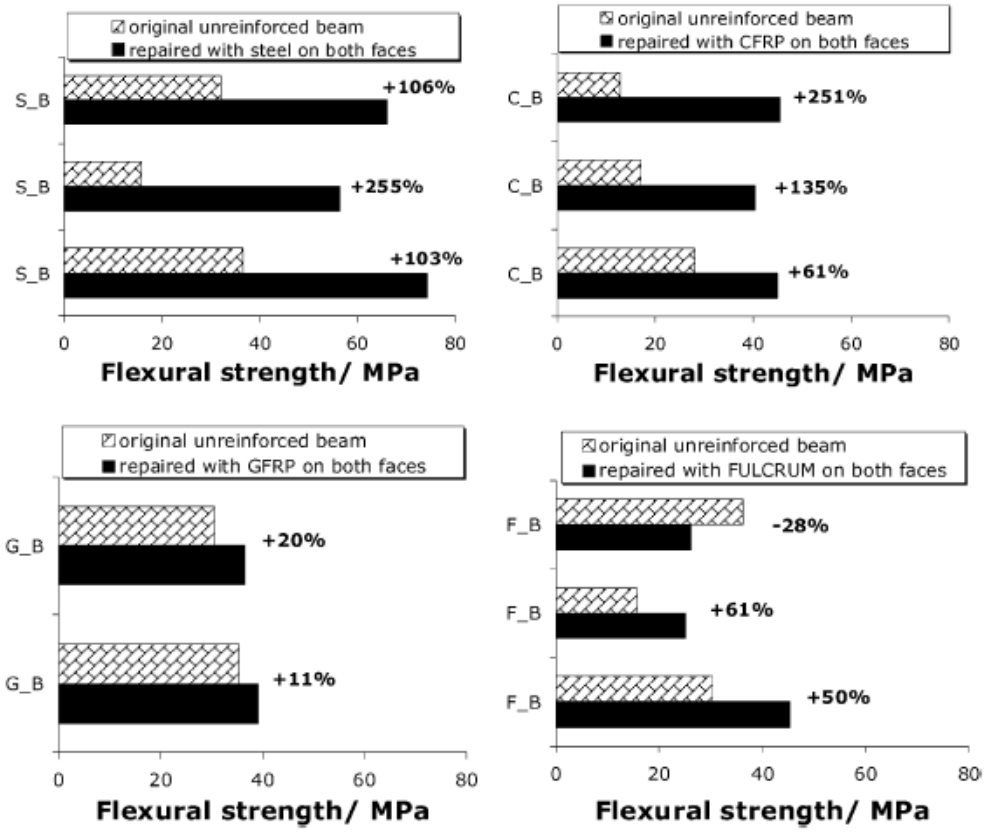

Figure 12: The variation in flexural strength of the beams repaired in both faces relatively to an undamaged beam **(5)**.

Campilho *et al*. (8) (7) (6) studied the repair of wood beams damaged by cross-grain tension, compression and horizontal shear. The wood beams were repaired by bonding CFRP patches. The three repair configurations are shown in figures [13-15].

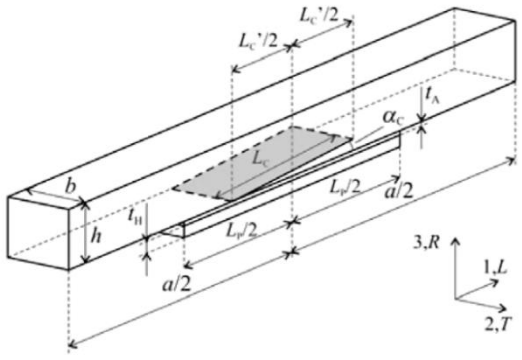

Figure 13:Schematic geometry of the cross grain tension repair specimen used by Campilho et al **(8)**.

.

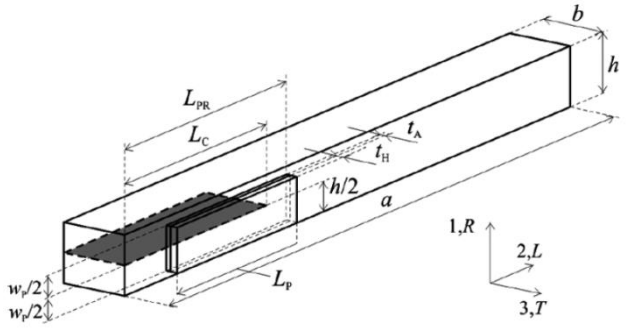

Figure 14: Schematic geometry of the horizontal shear repair specimen used by Campilho et al **(6)**.

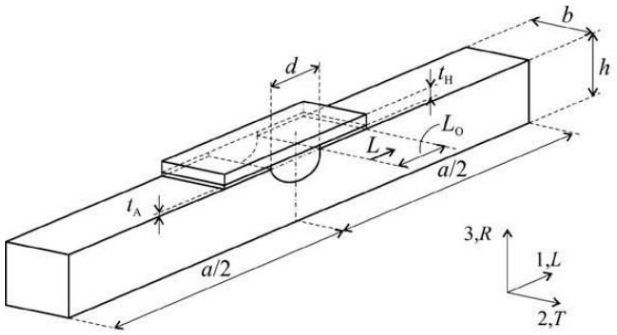

Figure 15: Schematic geometry of the compression specimen used by Campilho et al **(7)**.

All but the beams with horizontal shear cracks were experimentally tested under four point bending and the effectiveness of the patch length was analysed. All the repaired beams were simulated using the FEM and CZM. The results showed that the FEM and CZM can be used to predict the failure modes, elastic stiffness and maximum load of the repairs.

2.2 Adhesive Joints

2.2.1 Factors Affecting the Strength of Adhesive Joints

It is known that bonded joints provide a more uniform stress distribution than, for example, mechanical fasteners. However, there are still points at which peak stresses may occur, causing premature failure of the adhesive and reducing the joint strength, especially if brittle adhesives are used (9).

The main aspects that affect the strength of adhesive joints are the adhesive and the adherend mechanical properties and the geometry of the joint (9).

2.2.1.1 Adhesive Properties

The adhesive mechanical properties that affect the joint strength are mainly the adhesive strength, stiffness and ductility. Strong adhesives do not always provide strong joints as they do not distribute the stresses evenly. They are usually brittle and stiff, consequently very prone to stress concentration, resulting in a low average stress (9). On the other hand, ductile adhesives can provide a more uniform stress distribution, but are not as strong as brittle adhesives. Due to the higher damping properties of ductile adhesives, they are also more resistant to crack propagation, which makes them more resistant to fatigue cycles.

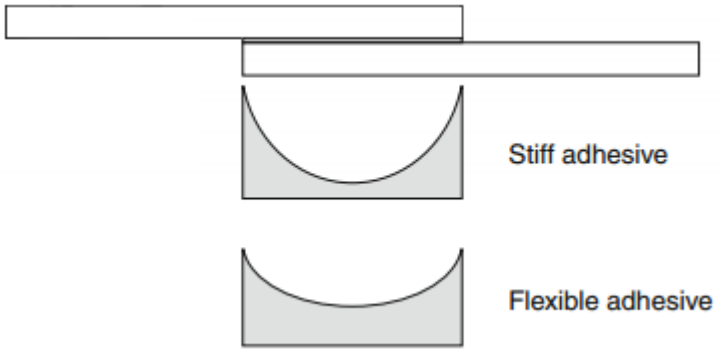

Figure 16: Stress distribution in a stiff adhesive and in a brittle adhesive **(9)**.

2.2.1.2 Adherend Properties

The main adherend properties that affect the strength of adhesive joints are the stiffness and the strength. The higher the flexibility of the adherends, the greater is the deformation of the overlap, resulting in a weaker joint (9). On the other hand, if weak adherends are used, plastic deformation in the edge of the overlap may occur, causing premature failure of the adhesive (9).

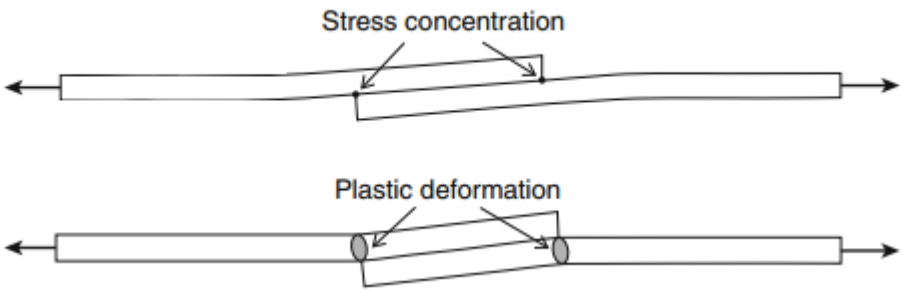

Figure 17: Yielding of the adherends **(9)**.

If orthotropic materials are used, such as CFRP, attention must be paied to the transverse strength of the material (through the thickness). It is recommendable that the outer layers of

the composite are aligned with the loading, otherwise it is likely fail in an interlaminar manner due to the peel stress (Figure 18) (9) (18). In order to reduce the peel stress, the stiffness should be locally reduced at the end of the overlap.

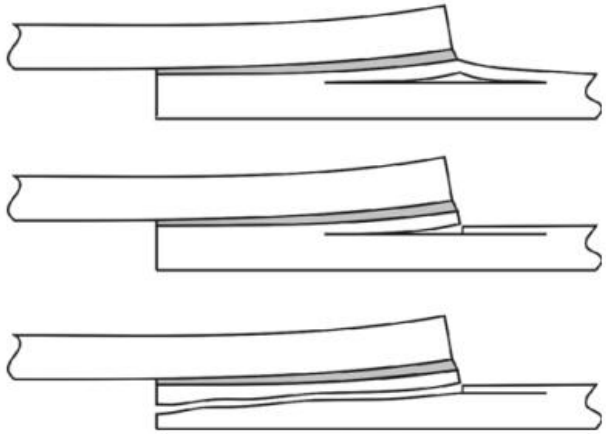

Figure 18: Interlaminar failure of a FRP adherend **(9)**.

2.2.1.3 Adhesive Thickness

Classical models such as those of Volkersen (19) or Goland and Reissner (20), which do not take into account the plasticity of the adhesive, predict that the strength of the joint increases with the adhesive thickness. However, experimental results show that the optimum bondline thickness is between 0.1 and 0.2 mm (9) (21). In order to understand this, some authors have proposed explanations.

Adams and Peppiatt (22) say that thicker joints have more defects, such as voids and microcracks and that these are responsible for the strength reduction in single lap joints.

Crocombe (23) explains that thinner bondlines have greater strength considering the plasticity of the adhesive. Thicker bondlines experience a more uniform stress distribution than thinner bondlines. However, when yielding occurs, thinner bondlines have more "elastic reserve", causing the yielding to spread more slowly and increasing the strength of the joint.

Da Silva *et al.* (24) have distinguished two types of plastification that can appear in single lap joints whith ductile adhesives: localized plastification (appears in the singular points and does not affect the P-δ curve) and globalized plastification (appears in a late stage of the test and changes the slope of the P-δ curve). da Silva *et al.* have found that in low thickness joints, the localized plastification occurs sooner and the globalized plastification occurs later than in high thickness joints. This helps explaining why low thickness joints are usually stronger than high thickness joints.

2.2.1.4 Overlap Length

In single lap joints, for example, peak stresses occur at the edges of the overlap. When rupture occurs, the stress concentration points are under the maximum stress while the middle of the overlap is underloaded (25) especially if the adhesive is stiff and brittle. This means that the total area of the overlap is not fully efficient. This phenomenon gets more critical if the overlap is long. In this case the stress may even become null, which means that if the length is further increased, no improvement will be achieved in the load bearing area and, consequently, on the strength of the joint (25) (Figure 19). This becomes critical if brittle adhesives are used.

If the adhesive is very ductile, the strength of the joint is approximately proportional to the overlap length, as it has the capability to deform and redistribute the stress evenly as the load increases (9).

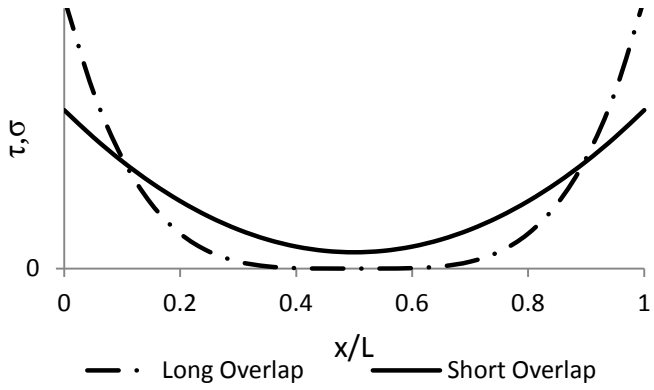

Figure 19: Typical stress distribution in a single lap joint

2.2.2 Methods to Increase Joint Strength

2.2.2.1 Spew Fillets

The spew is the portion of adhesive that is squeezed out of the lap as the two substrates are assembled (Figure 20). It is known that the stress concentration in the adherend-adhesive interface is reduced with the inclusion of these spews in the joint (26). The reduction in the stress concentration factor is function of the ductility of the adhesive and the adherend properties and also of the geometry of the spew (9) (27). Several spew geometries have been tested by Lang and Mallick (27), including triangular, full triangular, square, half rounded, full rounded, full rounded with fillet, oval and arc.

Despite being an efficient method to improve the strength of adhesive joints, in order to create spew fillets, several manufacture steps are required, thus increasing the cost of the bonding process. The use of this technique can also create more thermal stresses when used at low temperatures (9).

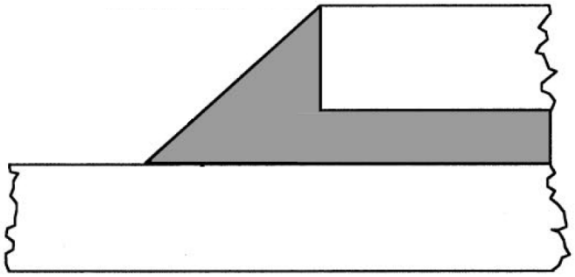

Figure 20: A triangular spew fillet.

2.2.2.2 Adherend Shaping

Adherend shaping can reduce the stress concentration at the edges of the overlap, strengthening the joint (Figure 21). If the stiffness of the joint in the stress concentration points is reduced, a more uniform stress distribution can be obtained (9) (18). This technique can also be combined with the use of spew fillets. Adherend shaping techniques such as internal or external tapers are efficient in reducing the peel stress in adhesive joints. This is very important especially when FRP adherends are used (18), as their transverse strength and consequently their resistance to peel stresses, are very low. Due to its high cost, this technique is often not possible to be used.

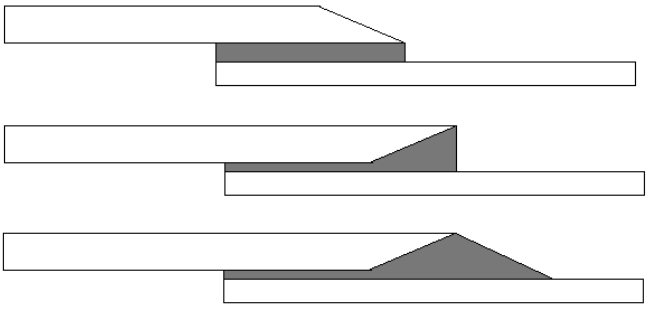

Figure 21: Different adherend shapes **(9)**.

2.2.2.3 Adherend Rounding

If the adherend corners are rounded (Figure 22), the stress in the singular points (points where the stress concentration factor is infinite), may be reduced, increasing the joint strength. This effect is only local, as the stress distribution away from the rounded area is not affected

(9). These singular points do not exist in practical, as the adherends are always slightly rounded in the manufacturing process.

This phenomenon has been studied by Adams and Harris (28), who found that the point of maximum stress is slightly dislocated away from the corner.

Zhao *et al*. (29) concluded that the improvement of the joint strength is smaller if ductile adhesives are used. Using a brittle adhesive an improvement in joint strength of 40% was achieved.

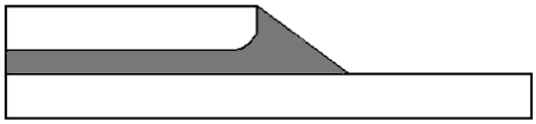

Figure 22: Adherend rounding **(9)**.

2.2.2.4 Mixed Adhesive Technique

A technique that is also used to reduce the stress concentration at the ends of the overlap is the mixed adhesive technique. Instead of using a single brittle adhesive along the entire overlap length, two adhesives are used. This second adhesive must be more flexible and is placed at ends of the overlap. This way, the stress at the edges of the bondlength, is decreased, resulting in a more uniform stress distribution and in a stronger joint (9) (30).

One disadvantage of this kind of joint is the adhesive separation. Despite being difficult to find compatible adhesives, the best way to control the process is still to use film adhesives. Another way to do this is to use silicon strips. However, if this technique is used, there is a small decrease in the load bearing area (9).

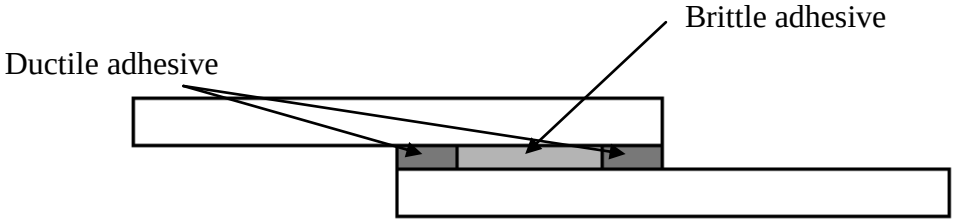

Figure 23: The mixed adhesive technique **(9)**.

2.2.2.5 Graded Materials

In order to decrease the stress concentration at the edges of the overlap, functionally graded materials can be used. The idea is to have an adherend or adhesive whose mechanical properties may vary along the bondlength. If the stiffness of the joint can be changed along the bondlength, a more uniform stress distribution can be obtained, thus strengthening the joint.

Apalak and Gunes (31) (32) and Gannesh and Choo (33) have used finite element analysis to simulate joints with functionally graded adherends, however, to the author's knowledge, no joint has ever been experimentally tested.

Stapleton *et al*. (10) studied the effect of functionally graded adhesives in single strap joints. Different concentrations of glass beads along the bondlength were used in order to create a gradient in the rigidity of the adhesive. A significant increase in the joint strength was achieved.

Carbas *et al* obtained a variable modulus bondline through the use of a graded cure. The graded cure, which allowed the adhesive to have different properties along the bondlength, was made with induction heating. A considerable increase in the strength of single lap joints was achieved. The adhesive was modified to show a gradient in the rigidity along the overlap, being its stiffness maximum at the middle and minimum at the ends. This modification was achieved with a differentiated cure process. The temperature of cure was not uniform along the entire bondlength, causing the adhesive to develop different mechanical properties along the overlap. In order to obtain different temperatures at the middle and at the end of the overlap, a special apparatus was invented (34). Single lap joints were tested with two different adhesives (Loctite Hysol® 3422 and Araldite® 2011) and with three different kinds of cure (35):

- Low temperature cure
- High temperature cure
- Graded Cure

The results showed that the graded cure was able to increase the strength of the graded Loctite Hysol® joint by 210% in relation to the joints cured at low temperature (brittle behaviour) and by 62% in relation to the joints cured at high temperature (ductile behaviour). The strength gain of the graded Araldite® joint was of 70% in relation to the high and low temperature cure (35).

2.3 Strength Prediction

2.3.1 Material Resistance Based Criteria

These criteria are based on the analysis of stresses and strains of the structures. With the help of the FEM or analytical models, it is possible to know the stress and displacement field around a certain point. However, real structures have points where the stress concentration factor tends to infinite. In these singular points, the solution provided by the FEM is highly mesh-dependent and not accurate. This kind of problem can be minimized with the use of the point stress criteria (36), in which the stresses are computed at a pre-defined distance from the singular point, and with the use of average stress criteria (36), in which an average stress is computed along a determined path.

2.3.2 Fracture Mechanics Based Criteria

Unlike the material resistance based criteria, the fracture mechanics based criteria have the ability to determine, taking into account the existence of singular points in the structure, when a crack may start to propagate.

There are two kinds of formulation in the fracture mechanics based criteria: The one based on the stress intensity factor (K) and the one based on the energy release rate (G).

2.3.2.1 The stress intensity factor

The stress intensity factor (K_i) is defined as:

$$K_i = Y\sigma_r\sqrt{\pi a} \tag{1}$$

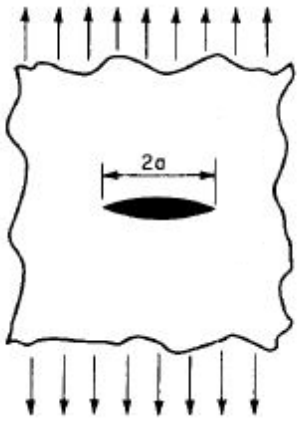

Figure 24: Mode I crack solicitation.

In which σ_r is the remote tension and a is the crack length (Figure 24). Crack propagation occurs as soon as K_i equals K_{iC}. K_{iC} is the critical stress intensity factor, a property of the material and a measure of its toughness. Y is a dimensionless correction factor that depends on the mode of solicitation and geometry. There are three pure modes of solicitation, as can be seen in Figure 25.

i) Mode I crack: Opening mode
ii) Mode II crack: Sliding mode
iii) Mode III crack: Tearing mode

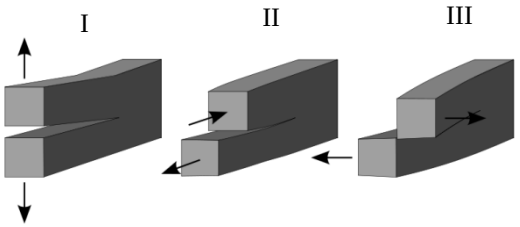

Figure 25: Modes of crack solicitation.

2.3.2.2 The energy release rate

The energy release rate is defined as:

$$G = \frac{dW}{dA} - \frac{dU}{dA} \tag{2}$$

W represents the work of external forces, U represents the deformation energy and A represents the area of propagated crack. As in the previous case, there is crack propagation when G equals G_C, the fracture energy, a property of the material.

The energy release rate is related to the stress intensity factor:

i) For plane stress:

$$G_I = \frac{K_I^2}{E} \tag{3}$$

ii) For plane strain:

$$G_I = \frac{K_I^2(1-\nu^2)}{E} \tag{4}$$

Where ν and E represent the Poisson's ratio and the Young's modulus respectively.

2.3.3 Cohesive Zone Models

These models have the advantage of combining the material resistance based criteria with fracture mechanics, accurately predicting the behaviour of the materials. CZM can predict the formation and propagation of cracks. (36)

As soon as, in a given node, the strength of the material is reached, softening initiates. Depending on the properties of the material, several cohesive laws can be used to simulate the softening of the material. These include triangular, linear-parabolic, polynomial, exponential and trapezoidal laws.

Although the cohesive laws can be adjusted to better fit the behaviour of the material, the triangular CZM, due to its simplicity, is very widely used and provides good results for most of the real situations (37). In this project, every simulation was carried out with the use of a triangular cohesive zone model (Figure 26).

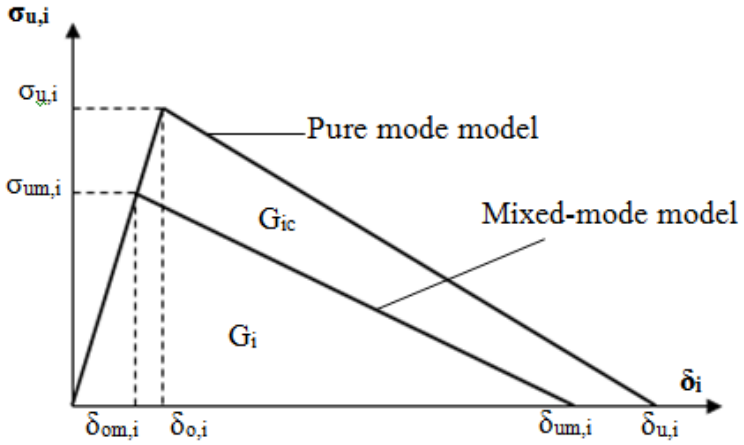

Figure 26: Triangular cohesive zone model.

The triangular cohesive law has an initial elastic behaviour. After the maximum stress is achieved, linear softening initiates. When the stress reaches the value of zero, no load can be transmitted, which is the same as saying that a crack has been created.

3 Characterization of the Adhesive

In order to obtain a functionally graded adhesive, a graded cure was used. This means that the adhesive must have different mechanical properties (particularly the stiffness and ductility) for different temperatures of cure. The greater the range of these properties, the more effective the graded joint can potentially be.

Carbas *et al*. (11) (38) studied the tensile properties of different epoxy adhesives as a function of the temperature of cure: Araldite 2011® (Huntsman, Basel, Switzerland), Araldite® AV 138M (Hunstman, Cambridge, England), Sikadur®-30LP (Sika, Zurich, Switzerland) and Locktite Hysol® 3422. Of these adhesives, the one with the widest range of Young's modulus is the Locktite Hysol® 3422 adhesive (Figure 27) and is therefore the one chosen for this project.

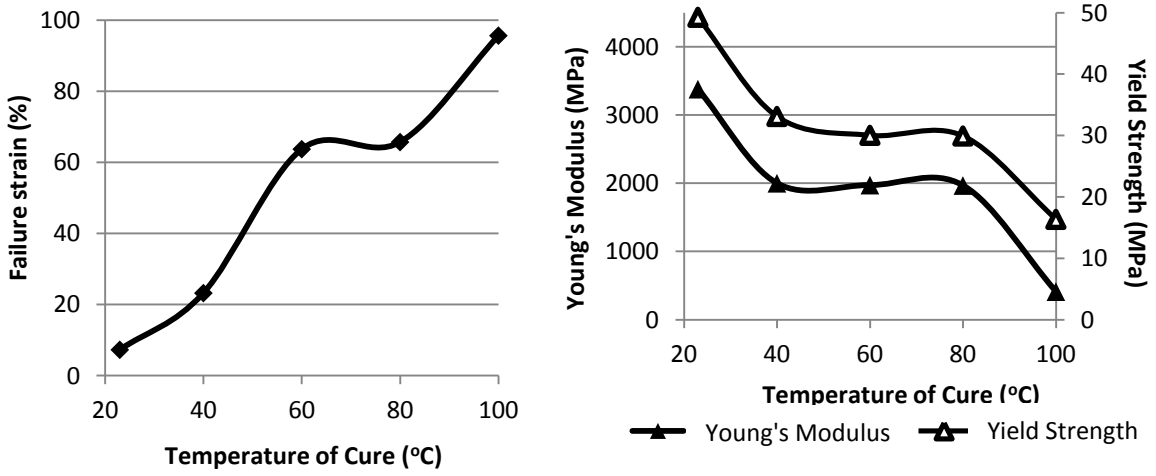

Figure 27 Mechanical properties of the Locktite® Hysol 3422 adhesive.

In order to accurately simulate the behaviour of the repaired wood specimens, the fracture toughness of the adhesive in pure modes I and II for three temperatures of cure was determined. For this, the DCB (pure mode I) and the ENF (pure mode II) tests were used.

3.1 Manufacture of the DCB and ENF specimens

Before the application of the adhesive, the surfaces of the adherends were grit blasted and degreased with acetone. In order to guarantee a 0.2 mm adhesive thickness, one spacer was inserted at each end. On the end where the crack is supposed to propagate, the spacer was constituted by a 0.1 mm razor blade inserted between two 0.05 mm plates. This allows the stress concentration factor to increase, making it easier for a crack to be created. The schematic geometry of the DCB and ENF specimens is represented in Figure 28. Its dimensions are shown in Table 1.

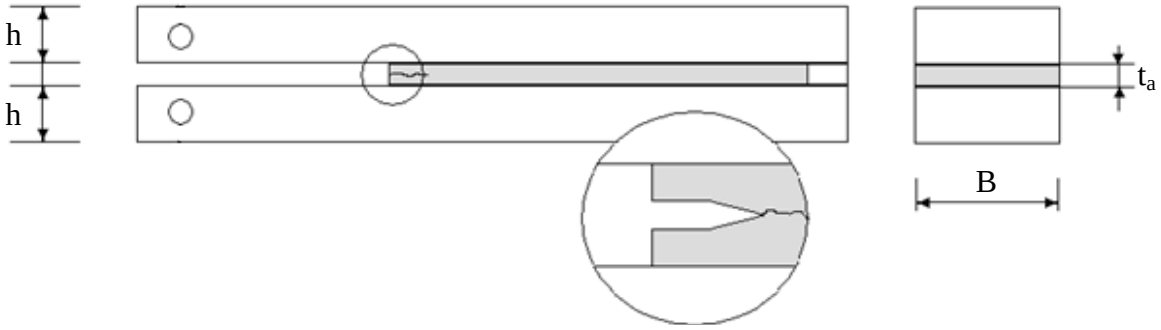

Figure 28: Schematic representation of the DCB and ENF specimens.

Table 1: Dimensions of the DCB and ENF specimens

h	B	t_a
12.7 mm	24.8 mm	0.2 mm

The specimens were placed in a mould inside a hot plates press for correct alignment. They were then subjected to a heat and pressure cycle that is necessary to cure the adhesive and eliminate bubbles and other defects (Figure 29). Three different temperature of cure (23^{o}C, 60^{o}C and 100^{o}C) were used, so that its influence in the toughness of the adhesive could be assessed. After this, the spacers were removed, along with the excessive adhesive. Prior to the testing of the specimens, in order to avoid a blunt crack; a 15 to 20 mm pre-crack was created by loading each specimen in pure mode I.

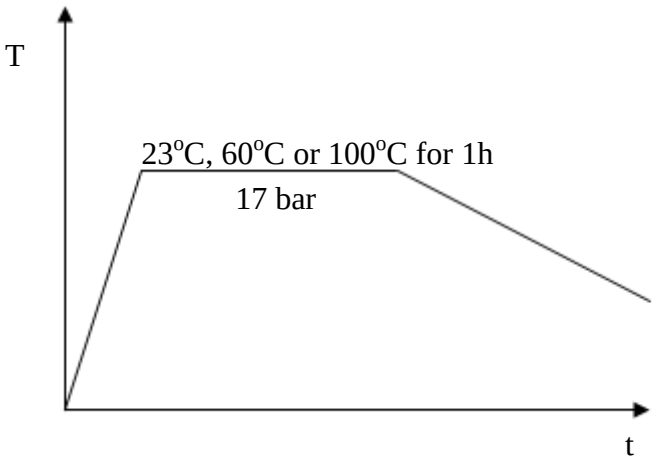

Figure 29: Different cure cycles of the adhesive.

3.2 Pure Mode I Toughness

The determination of G_{IC} was done with the use of DCB specimens. This test consists on the mode I solicitation of the adhesive. During crack propagation, the values of load (P) and displacement (δ) are recorded. In order to calculate the fracture toughness, the compliance based beam method (CBBM) was used. This is a technique that has recently been developed by de Moura *et al*. (12) (39).

The great advantage of this method is that it does not require the measurement of the crack length during propagation. An equivalent crack length is computed based only on the specimen's compliance during the test (12). This approximation based on the Timoshenko beam theory makes it possible to know the crack length based on the compliance of the specimen during the test. The crack length that is calculated using this method is an equivalent crack length, as it also takes into account the length of the fracture process zone (Figure 30).

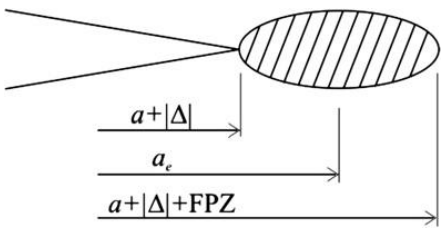

Figure 30: The crack tip and the fracture process zone.

3.2.1 Results

The specimens were tested in a MTS® model 312.31 servo-hydraulic with a capacity of 250 kN (Eden Prairie, Minnesota, USA) at room temperature.

The specimen with the adhesive cured at room temperature was tested at a displacement rate of 0.1 mm/min, however, due to the brittleness of the adhesive, unstable crack propagation was observed in all specimens, making it impossible to determine the mode I fracture toughness.

The specimens with the adhesive cured at 60°C and 100°C were tested at a displacement rate of 0.2 mm/min.

Bellow, are shown the *P-δ* curves and R-curves for the 60°C and 100°C cure

3.2.1.1 60°C Cure

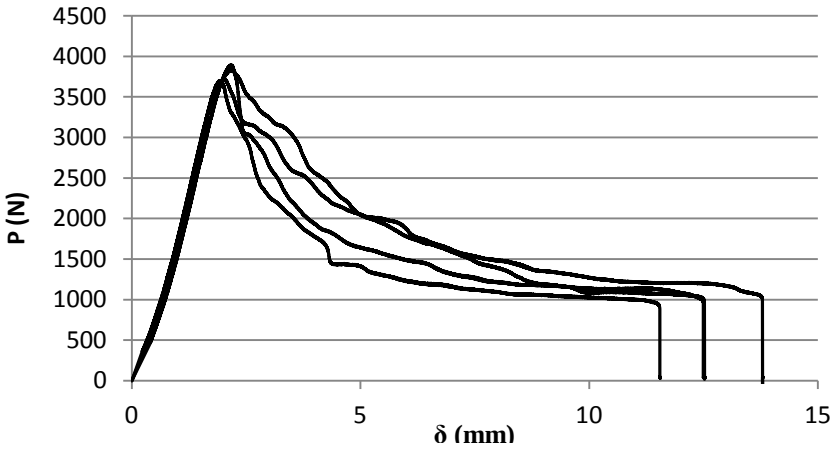

Figure 31: P-δ Curves of the 60°C cure DBC specimens.

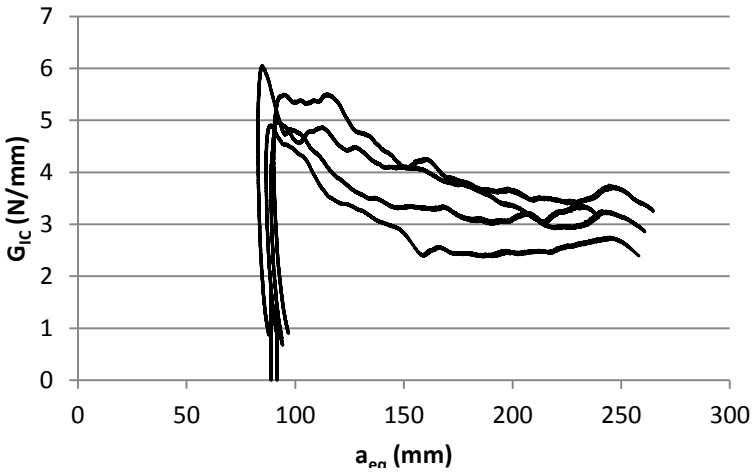

Figure 32: R-Curves of the 60°C cure DBC specimens.

3.2.1.2 100°C Cure

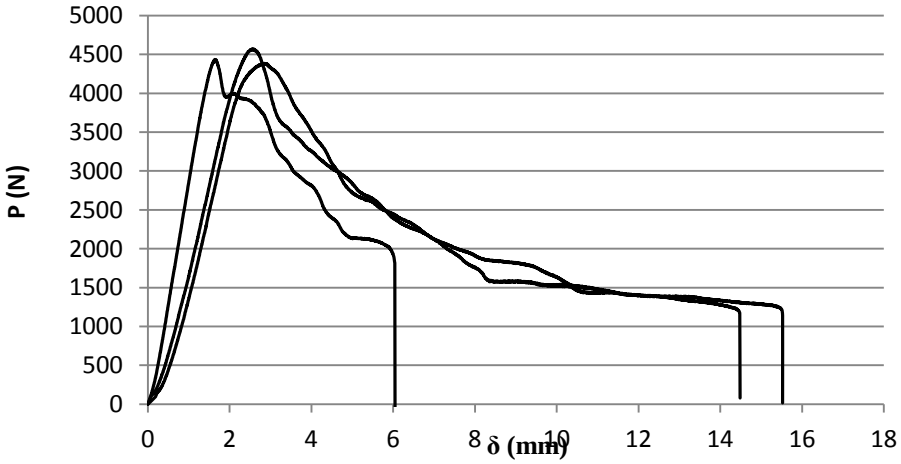

Figure 33: P-δ Curves of the 100°C cure DBC specimens.

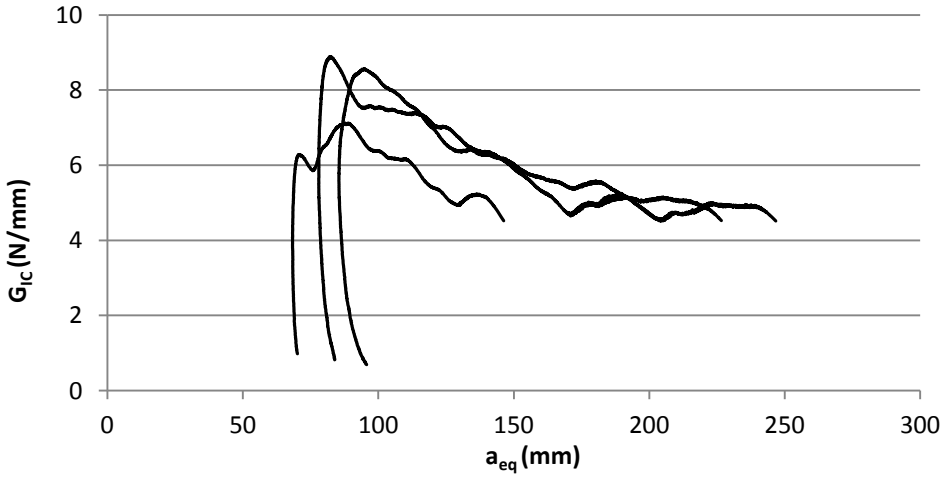

Figure 34: R-Curves of the 100°C cure DBC specimens

The mode I fracture energy of the adhesive cured at 100°C and 60°C was about 4,90 N/mm and 3.08 N/mm respectively, which is consistent with the studies made by Carbas *et al* (38). As the adhesive is fragile if cured at room temperature, despite a low test rate has been used, unstable crack propagation was observed, not allowing the determination of the mode I fracture energy.

3.3 Pure Mode II Toughness

The determination of G_{IIC} was done with the use of ENF specimens.The schematic geometry of the specimens used is shown in Figure 35. Two steel adherends are adhesively bonded and tested under three point bending. This allows the adhesive to be under a pure mode II solicitation. During crack propagation, the values of force (P) displacement (δ) are recorded.

In order to calculate the critical energy release rate in mode II, G_{IIC}, the CBBM was used. This method has recently been developed by de Moura *et al* (40) (13). In this method, an equivalent crack length is computed based only on the P-δ curve during the crack propagation, which means the crack length measurement during the test is not required.

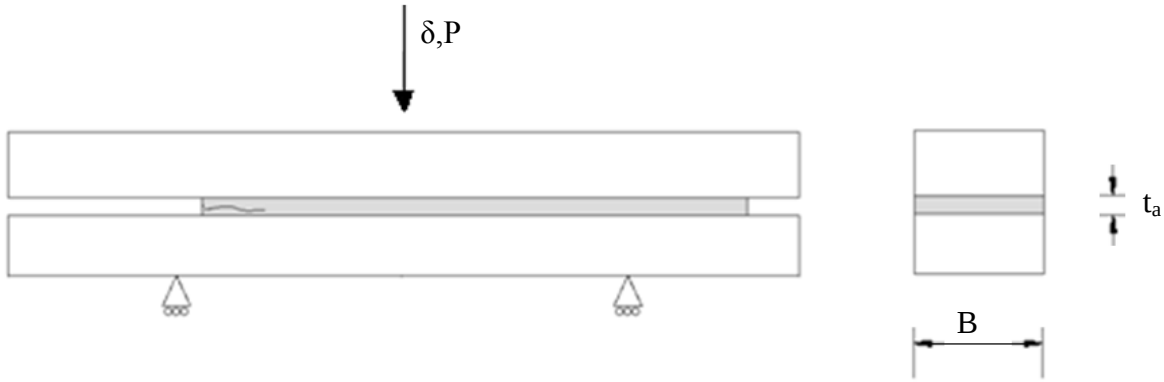

Figure 35: Geometry of the ENF specimens.

Table 2: Dimensions of the ENF specimens.

t_a=	0.2 mm
B=	24.8 mm

3.3.1 Results

The specimens were tested in a INSTRON® model 3367 universal test machine with a capacity of 30kN (Norwood, Massachusetts, USA), at room temperature and constant displacement rate of 0.5 mm/min.

For the 60°C and 100°C cure, due to the high ductility of the adhesive, the crack did not propagate. For this reason, no information could be recovered about the mode II fracture toughness of the adhesive.

Bellow are shown the results concerning the specimens with the adhesive cured at 23°C.

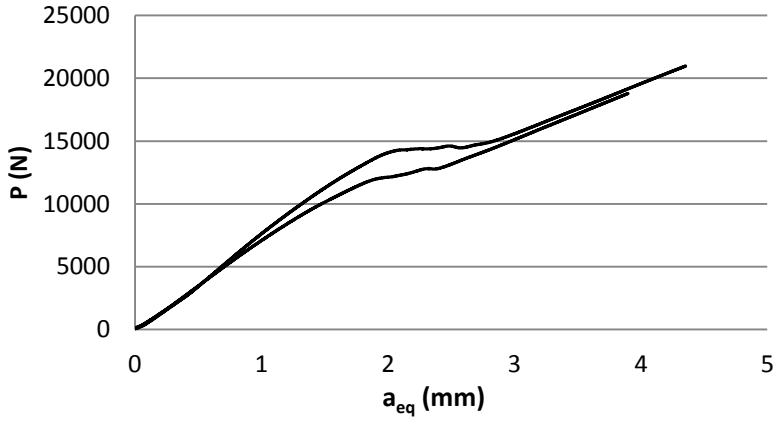

Figure 36: P-δ Curves of the 23°C cure ENF specimens.

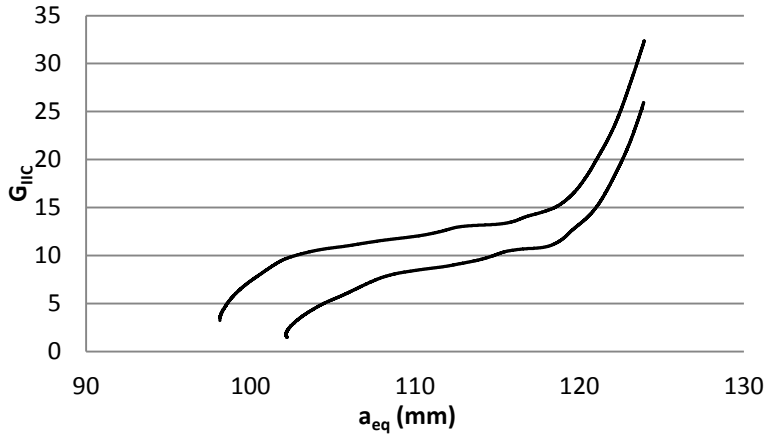

Figure 37: R-Curves of the 23°C cure ENF specimens.

The results show that the mode II fracture toughness of the adhesive cured at 23°C is about 12.47 N/mm. Due to the high toughness of the adhesive when cured at 60°C and 100°C, G_{IIC} could not be determined.

3.4 Summary of Results

Table 3 summarizes the fracture toughness of the Locktite® Hysol 3422 adhesive in modes I and II, which were used in the repaired wood specimens simulations. Since the mode I toughness of the adhesive cured at 23°C and the mode II toughness of the adhesive cured at 60°C and 100°C could not be determined, these values were extrapolated and are written in bold.

The values are graphically represented in Figure 38.

Table 3: Fracture Toughness of the adhesive in modes I and II.

Temperature of Cure (^{o}C)	G_{IC} (N/mm)	G_{IIC} (N/mm)
23	**1.40**	12.47±0.71
60	3.08±0.10	**15.40**
100	4.90±0.08	**19.60**

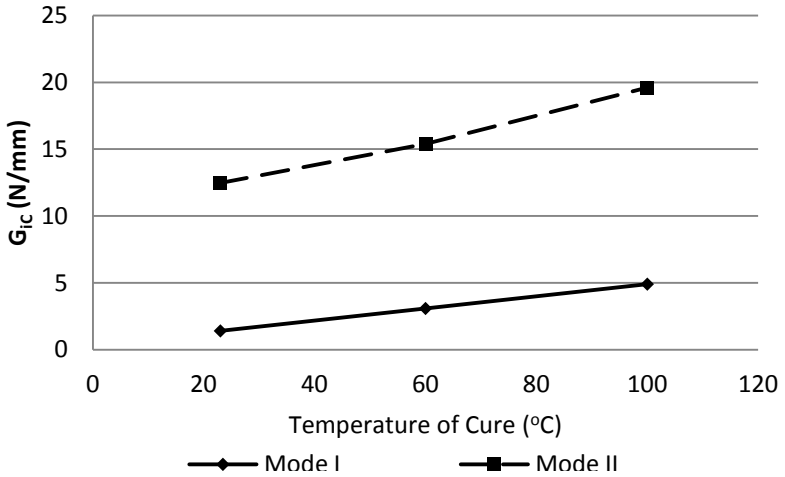

Figure 38: Toughness in modes I and II as a function of the temperature of cure.

4 Repair of Wood Structures

4.1 Mechanical Properties of the *Pinus Pinaster* Wood

On the macroscopic scale, wood is an orthotropic material with three orthogonal directions of symmetry (41) (42) (40) (Figure 39):

- L, the longitudinal direction;
- R, the radial direction of the annual rings;
- T, the tangential, direction of the annual rings.

Six propagation systems are distinguished for each propagation mode (I, II and III): TL, RL, LR, TR, RT, and LT (42) (40) (Figure 40). The first letter refers to the normal direction to the crack plane and the second letter to the direction of crack growth.

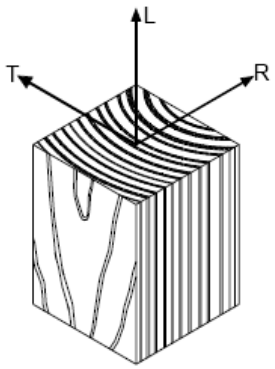

Figure 39: Orthogonal directions of symmetry of wood **(41)**.

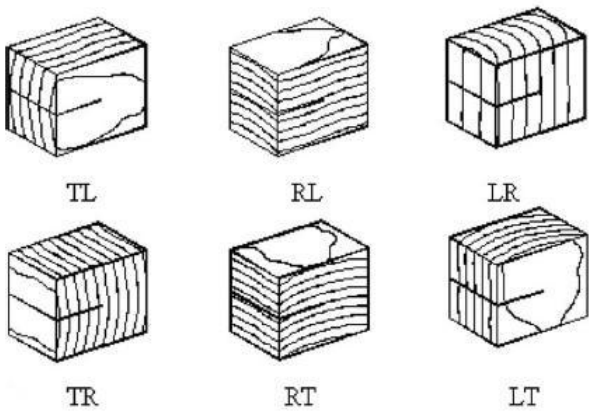

Figure 40: Crack propagation systems of wood.

Wood failure in two propagation systems in modes I and II were considered. The elastic and fracture properties of the *Pinus Pinaster* wood are in Table 4and Table 5 respectively. Because wood is a biological product, these values vary greatly from specimen to specimen, depending on the environment the tree grew in, among other factors.

Table 4: Elastic properties of the *Pinus Pinaster* wood **(40)**.

E_L=15.13 GPa	ν_{LR}=0.47	G_{LR}=1120 MPa
E_R=1910 MPa	ν_{LT}=0.51	G_{LT}=1040 MPa
E_T=1010 MPa	ν_{RT}=0.59	G_{RT}=170 MPa

Table 5: Cohesive properties of the *Pinus Pinaster* wood for two propagation systems **(43)**.

	RL Plane		LR Plane	
Pure mode	I	II	I	II
$\sigma_{u,i}$ [MPa]	16	16	65	16
G_{iC} [N/mm]	0.2	1.2	25	1.2

4.2 Geometry

Scaled specimens of *Pinus Pinaster* beams were repaired with bonded CFRP patches and tested under bending. These specimens were designed to simulate two common types of failure of wood beams under bending loads: compression failure (Figure 41) and cross grain tension failure (Figure 42). Table 6 shows the dimensions of the specimens.

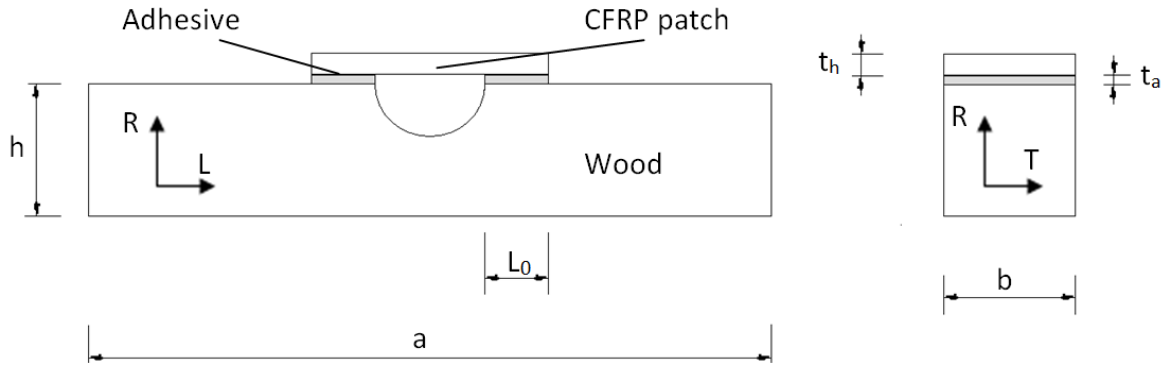

Figure 41: Schematic representation of the compression damage specimen.

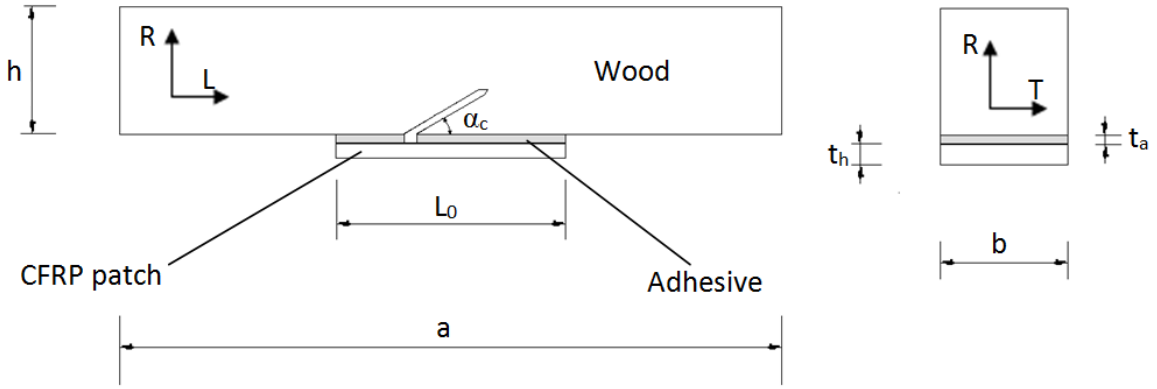

Figure 42: Schematic representation of the cross grain tension specimen.

The specimens were loaded under 4PB, as demonstrated in Figure 47.

Table 6: Geometry of the compression and cross grain tension specimens.

Compression failure specimen			
a=300 mm	b=20 mm	h=20 mm	t_a=0.2 mm
t_h=1.2 mm			
Cross grain tension failure specimen			
a=300 mm	b=20 mm	h=20 mm	t_a=0.2 mm
t_h=0.6 mm	α_c=15^o		

This specimen geometry is the same used by Campilho *et al*. (8) (7). For each kind of beam damage, two bonded lengths were considered (L_0): 20 and 30 mm for the compression damage and 40 and 60 mm for the cross grain tension damage.

4.3 Specimens Manufacture

Right before the bonding of the patches, in order to raise the critical surface tension of wood and improve its wettability, the wood surface was abraded with sandpaper and cleaned with compressed air. It was not cleaned with acetone, as it could be absorbed and affect the bonding.

The patches were also abraded with 220 grit sandpaper and cleaned with acetone. They were bonded using the Locktite Hysol® 3422 adhesive cured in three different ways:

- **Isothermal cure at room temperature (23^{o}C):** this allows the adhesive to have a stiff, brittle and high strength behaviour;
- **Isothermal cure at high temperature (100^{o}C):** this allows the adhesive to have a ductile, flexible and low strength behaviour;
- **Graded cure:** this allows the adhesive to be stiff where stresses are normally low and flexible where stresses are normally high. This way a more uniform stress distribution can be obtained.

4.3.1 Isothermal Cure

In order to guarantee the correct adhesive thickness, two spacers were used (Figure 43). The pressure was applied through the use of grips. Many specimens can be made with the use of a single pair of grips (Figure 44). This allows several specimens to be made at the same time.

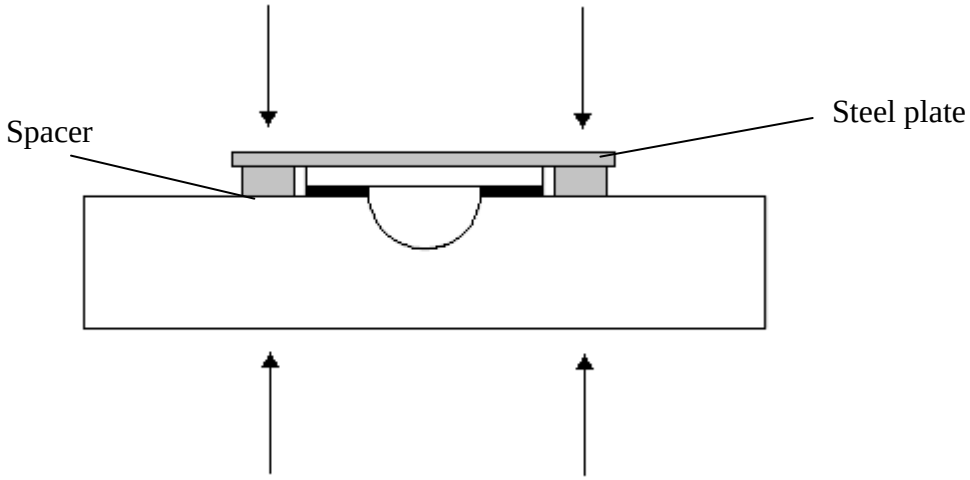

Figure 43: Way to guarantee the adhesive thickness.

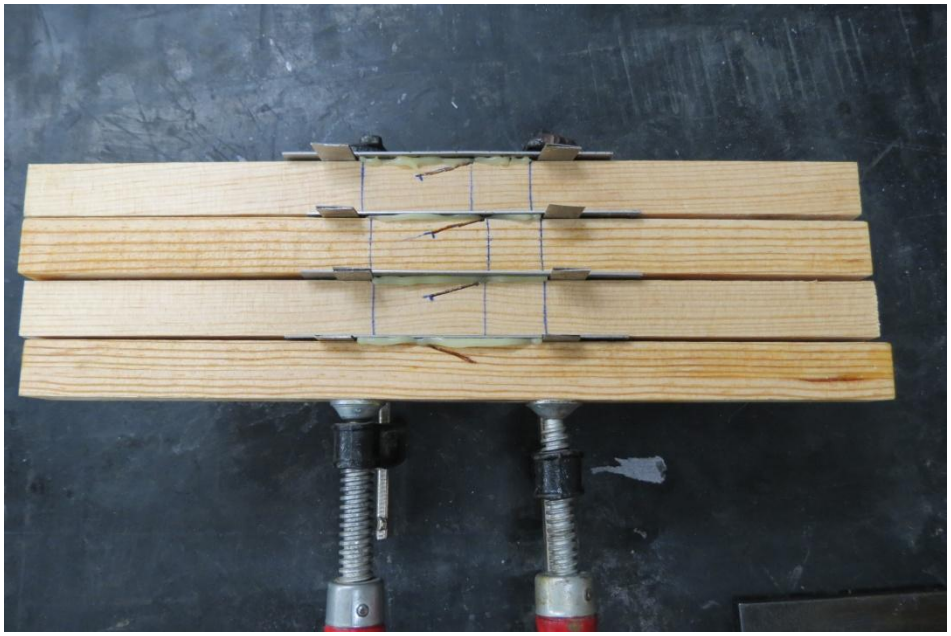

Figure 44: Several specimens being held by one pair of grips.

The specimens were left to cure either at room temperature (low temperature) or in the oven (100°C temperature of cure).

One week after the application, the excessive adhesive was removed.

4.3.2 Graded Cure

Induction heating was used to raise the temperature of the adhesive at the ends of the overlap, where the stress concentration exists. As this adhesive is flexible when cured at high temperatures, this allows the stresses in the joint to be more uniform. This technique has already been successfully used in single lap joints by Carbas *et al.* (35). A recently invented apparatus was used to locally heat the adhesive and perform a graded cure (34).

Figure 45 shows the approximated distribution of temperature along the overlap length for the compression and cross grain tension specimens. The temperature was monitored using a thermographic camera.

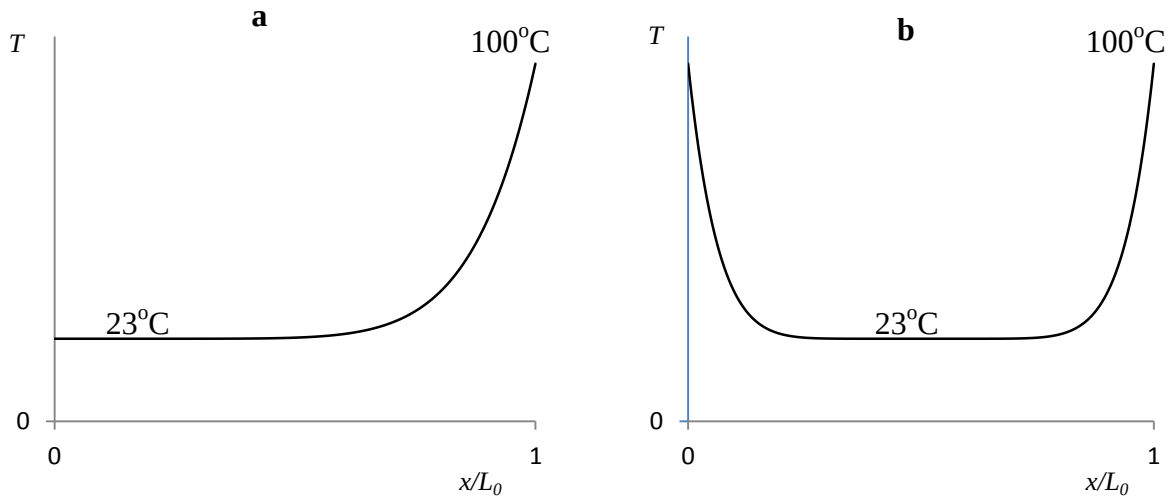

Figure 45: Approximated temperature distribution during the graded cures:

a. Compression specimens (half of the beam)
b. Cross grain tension specimens

As at ends of the overlap there is a greater gradient in the stress than in the middle. In order to obtain a more uniform distribution, these areas must also receive a considerable gradient in the rigidity. To achieve this, a great gradient in the temperature of cure was used at this area. At the middle of the overlap there is not a great variation in the stress. This is why a small gradient in the temperature of cure was used here.

4.4 Manufacture of the CFRP Patches

The wood beams were repaired using CFRP patches. This is an orthotropic material, whose elastic mechanical properties can be seen in Table 7.

Table 7: Elastic properties of the CFRP patches **(25)**.

E_x= 1.09E5 MPa	v_{xy}=0.342	G_{xy}=4315 MPa
E_y=8819 MPa	v_{xz}=0.342	G_{xz}=4315 MPa
E_z=8819 MPa	v_{yz}=0.380	G_{yz}=3200 MPa

Two 300x300 mm^2 CFRP plates were manufactured (one was 1.2 mm thick for the compression specimen, the other was 0.6 mm thick and was used in the repair of the cross grain tension specimen).

The manufacture process had five steps:

1. Cutting the pre impregnated carbon fibres in squares (300x300 mm^2). Each square becomes a layer. Each layer is 0.15 mm thick. For the 0.6 mm thick plate, four layers are needed and for the 1.2 mm thick plate, eight layers must be cut.
2. The Teflon® films involving the pre impregnated carbon fibre should be removed. Each plate should be placed on the top of the other. In this step attention must be paid to the orientation of the fibres. A hot air gun should be used to heat up the plates and activate the epoxy resin. The air bubbles that are created can be removed with the use of a heavy trowel.
3. Using duct tape, a steel strip with the thickness of the plate was attached perpendicular to the fibres. This prevents the deformation of the plate during the pressure cycle, as well as the resin loss.
4. The plate was subjected to the heat and pressure cycle illustrated in Figure 46. This was made using a hot plates press. It is very important that the cooling is slow, avoiding the formation of residual stresses.
5. After the cure of the epoxy resin, the plate was cut into the CFRP patches. This was done with a diamond tip saw.

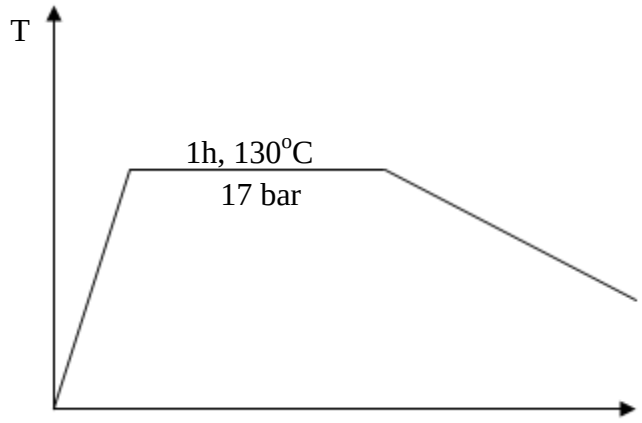

Figure 46: Thermal cycle of the CFRP plates.

4.5 Specimens Testing

The specimens were tested under four point bending in an INSTRON® model 3367 universal test machine with a capacity of 30kN. This allows a constant bending moment to be created on the repaired area (at the middle of the beam), as is shown in Figure 47. The displacement rate was 2 mm/min. The specimens were placed with the repaired area at equal distances from the rollers. The compression specimens had the patch on the upper side (compression face of the beam) and the cross grain tension specimens were placed with the repaired area on the bottom side of the beam (tensile face).

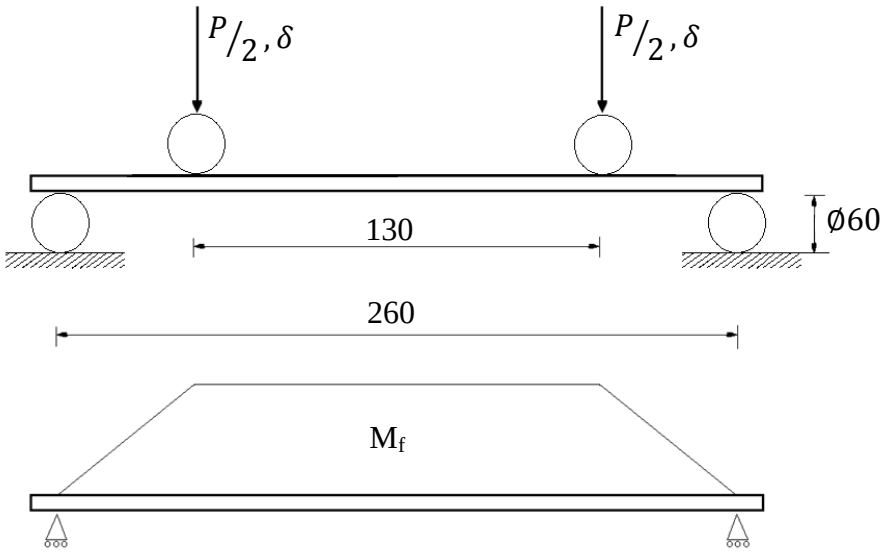

Figure 47: Bending moment (M_f) of a beam under four point bending.

Large rollers (60 mm in diameter) were used not to damage the wood beams. If small rollers had been used, indentation would have been created on the beams, affecting the P-δ curves. Five specimens were manufactured for each repair geometry. Only the valid tests were considered in the analysis of results.

4.6 Numerical Analysis

The FEM analyses were performed in Abaqus® using CZM. 2D models were used. The CFRP patch and the wood beam were modelled with 4 node solid elements (CPS4R). The adhesive was modelled with 4 node cohesive elements (COH2D4). Cohesive layers were also added to the beam (Figure 48), so that the crack initiation and propagation could be simulated.

Due to the symmetry of the compression specimen, in order to decrease the computational effort, only half of the beam was numerically simulated.

The boundary conditions, as well as the place where each layer of cohesive elements was created are represented in Figure 48.

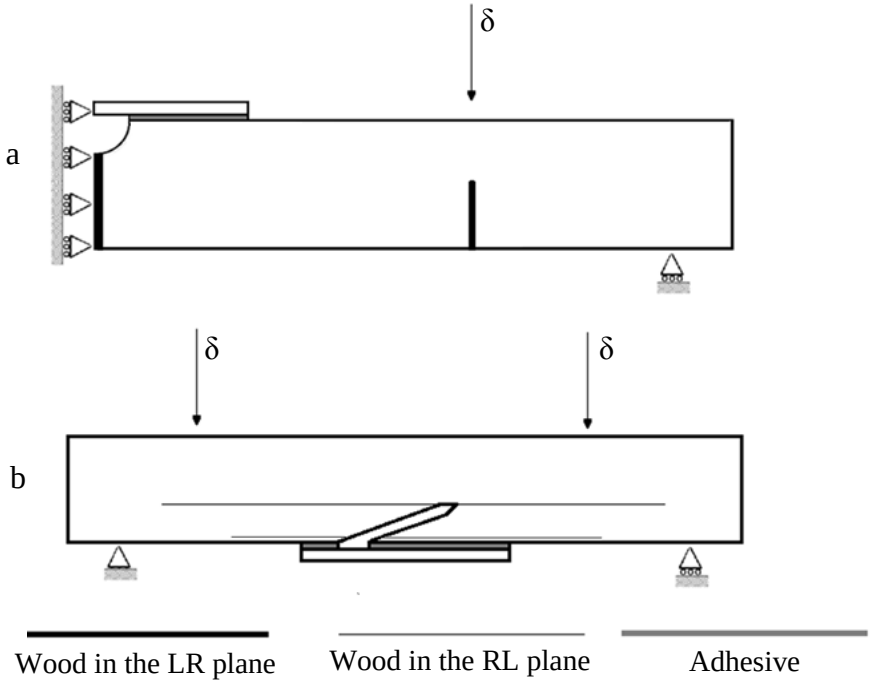

Figure 48: Boundary conditions and cohesive elements location:

a. Compression failure
b. Cross grain tension failure

In the compression specimens, to simulate failure at the symmetry axel of the beam and bellow the loading cylinder, cohesive layers of wood were added to these locations. In the

cross grain tension specimens, cohesive layers of wood in the RL plane were used in order to simulate the propagation of the pre-crack and the failure of the wood-adhesive interface. In all cases cohesive elements were used in the adhesive

The meshes used are illustrated in Figure 49 and Figure 50. The areas bearing greater stress gradients received a more refined mesh.

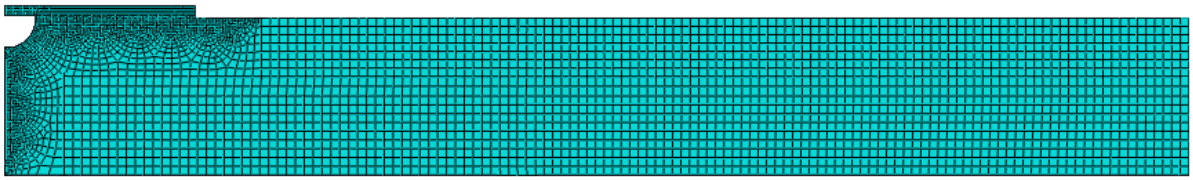

Figure 49: Mesh of the compression failure repair.

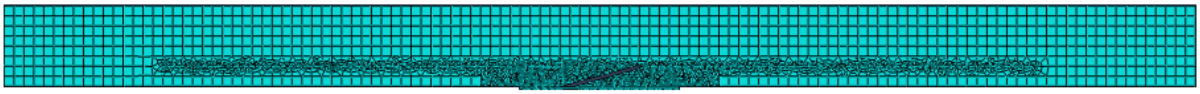

Figure 50: Mesh of the cross grain tension repair.

In order to simulate graded adhesive properties, several partitions were made in the adhesive layer. Different properties were assigned to each partition. These are the properties of the adhesive cured at different temperatures. This way it was possible to create an approximation to a graded bondline.

Figure 51 shows the partitions made in the adhesive for a compression damage specimen. In Figure 52 is a schematic representation of the Young's modulus of the adhesive in the numerical model along the overlap length. A considerable gradient in the stress exists s at ends of the overlap. These areas received a greater gradient in the rigidity, so that the stress distribution could be as uniform as possible. At the middle of the overlap there is not a great variation in the stress. This is why a small gradient in the rigidity was assigned to this area.

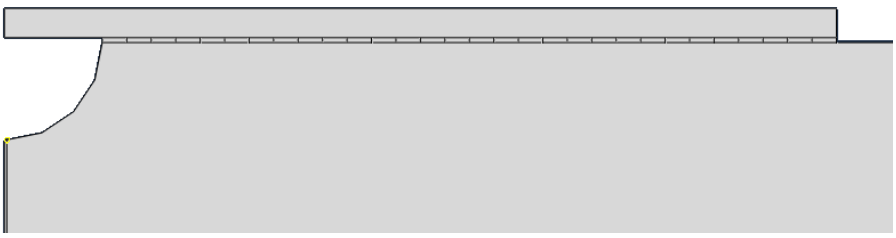

Figure 51: Several partitions in the adhesive layer were made in order to simulate graded properties.

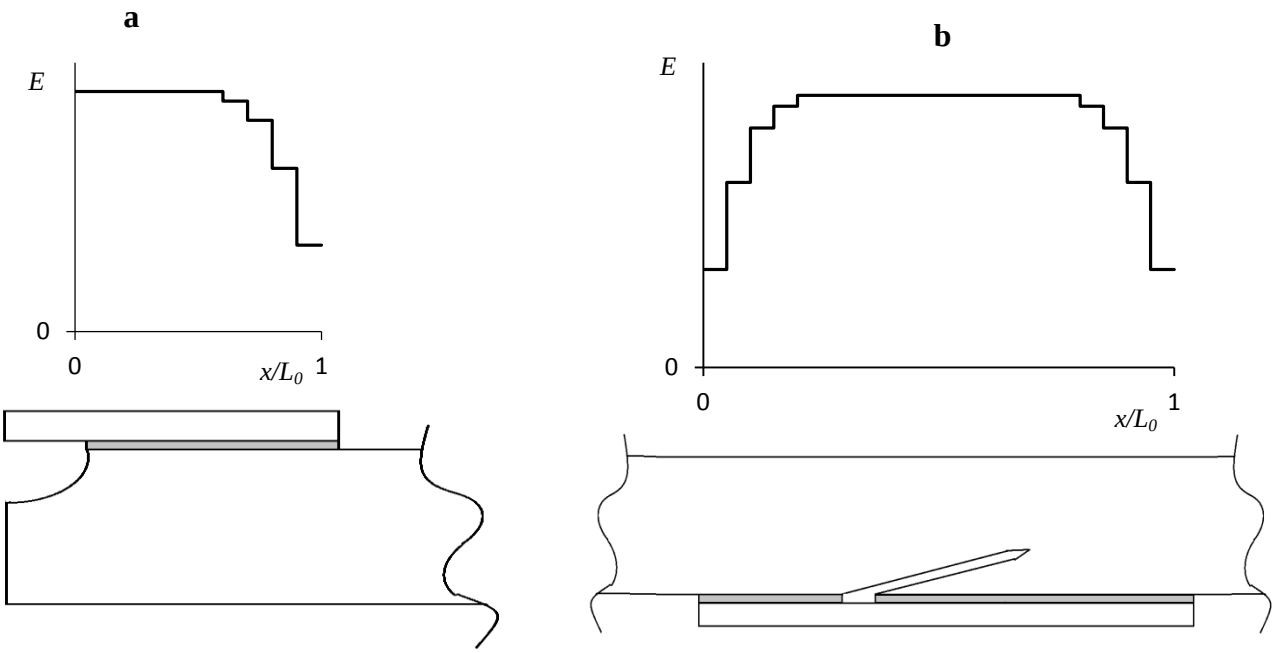

Figure 52: Schematic representation of the Young's modulus along the overlap length:

a- Compression specimens (only half of the beam was considered)
b- Cross grain tension specimens

However, this is not a perfect approximation. The stress distribution that is computed, as a result of discontinuous adhesive properties along the overlap, is not a continuous line. For this reason, the stress distributions regarding the graded cures were approximated by a six degree polynomial function. The shear stress distribution of the 20 mm compression specimen can be seen in Figure 53.

.

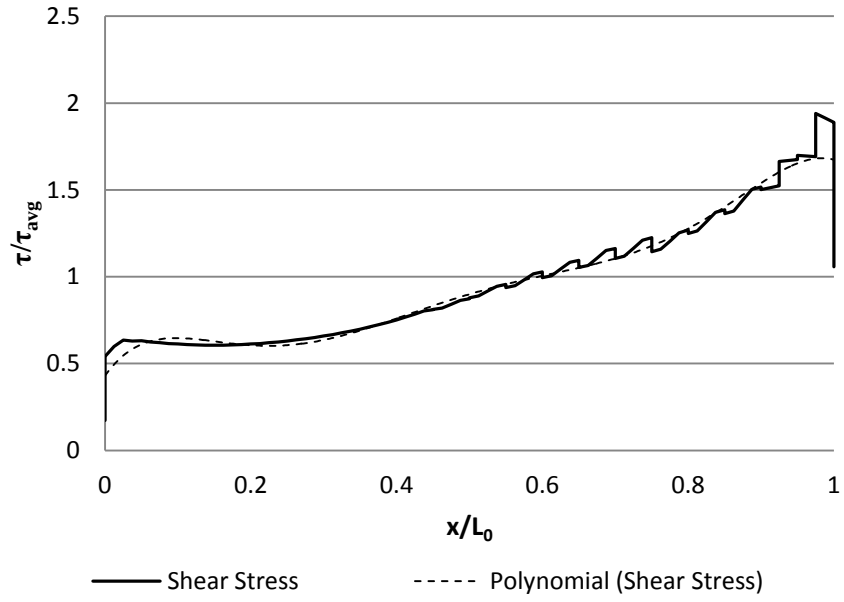

Figure 53: Numerical distribution of the shear stress in a graded joint.

4.6.1 Stress Distributions in the Adhesive Layer

In this section the stress distribution in the adhesive (shear and peel) in the compression and cross grain tension specimens under 4PB are presented. All the figures refer to the elastic domain.

4.6.1.1 Compression Specimens

Figure 54 and Figure 55 show the adimensionalised shear and peel stress $\left(\tau/\tau_{avg}\right.$ and $\left.\sigma/\tau_{avg}\right)$ of the compression specimens over the overlap length.

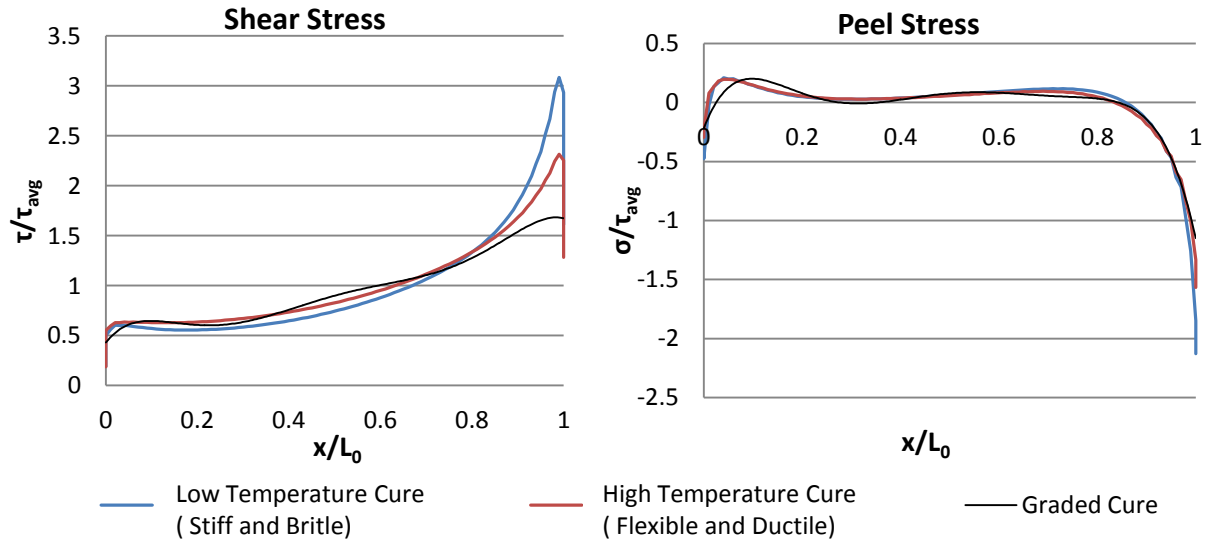

Figure 54: Shear and peel stress distribution in the 20 mm repair compression specimen.

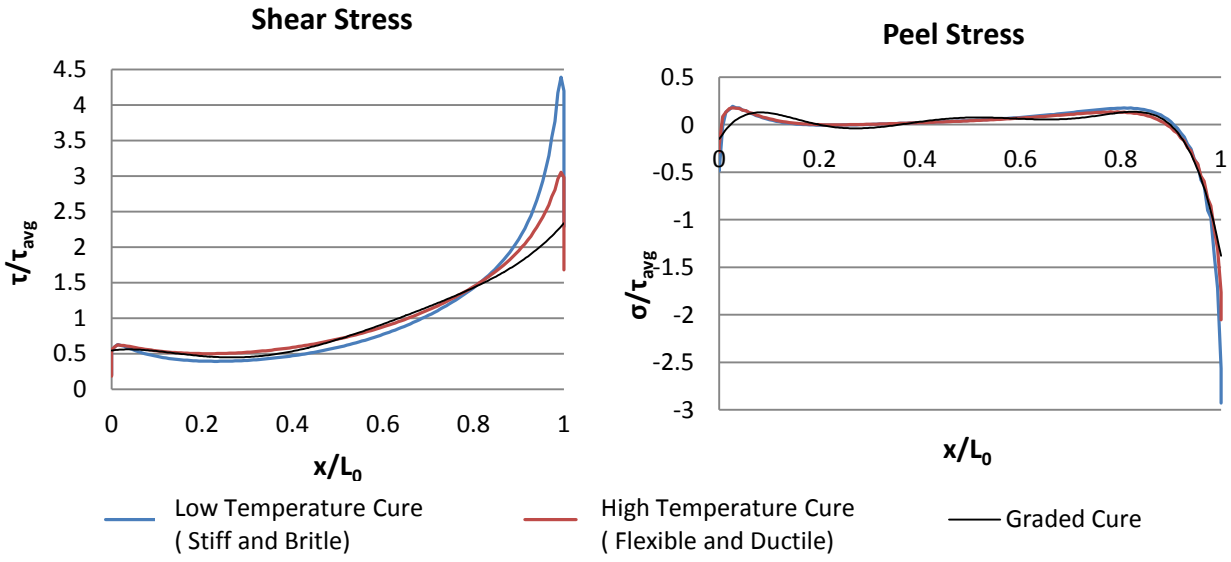

Figure 55: Shear and peel stress distribution in the 30 mm repair compression specimen.

In the repaired compression specimens, both the peel and the shear stresses are maximum at the ends of the overlap.

The longer the patch is, the greater are the adimensionalised shear and peel stresses. This is due to the less uniform stress distribution in longer overlaps. For the **same average shear stress**, the peaks at the ends of the overlap are higher in the long overlap. However, if both joints are under the **same load**, the true peak stress at the end of the long overlap must obviously be lower in the long overlap (as a consequence of its bigger resistant area and lower average shear stress).

The highest stress concentration factor belongs to the adhesive cured at room temperature, as its Young's modulus is the highest. If this adhesive is cured at 100°C, its Young's modulus gets lower, and is able to provide a more uniform stress distribution.

The graded cure was able to significantly decrease the stress concentration factor at the ends of the overlap when compared with the adhesive cured at high and low temperature.

4.6.1.2 Cross Grain Tension Specimens

Figure 56 and Figure 57 show the stress distribution along the overlap for the cross grain tension repairs.

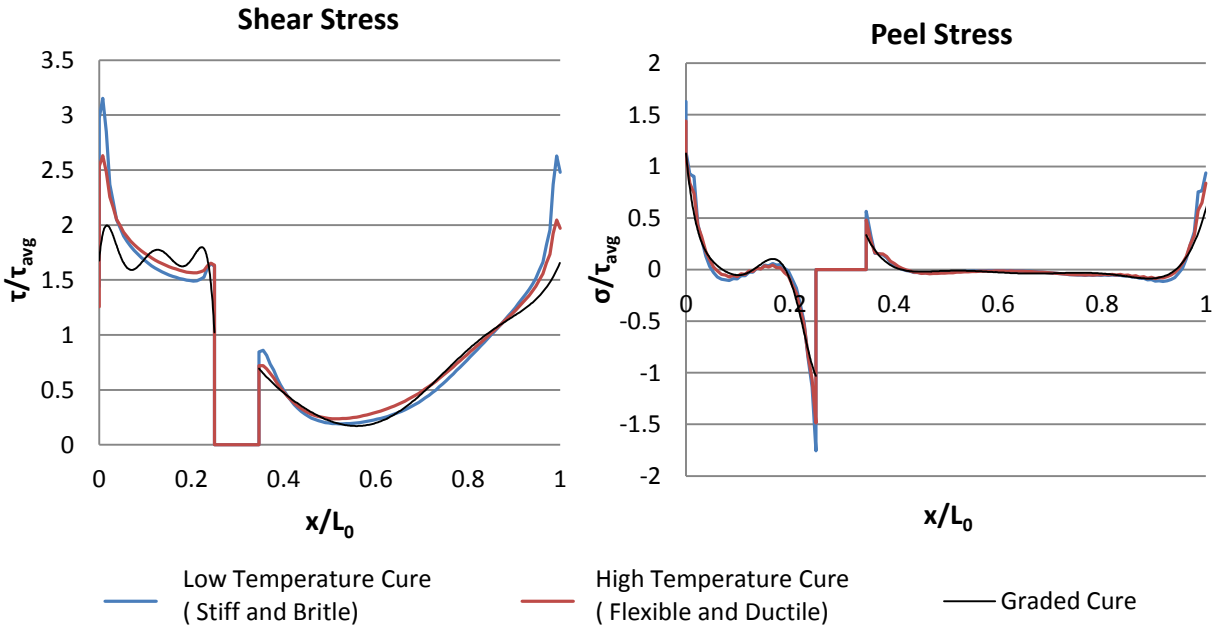

Figure 56: Shear and peel stress distribution in the 40 mm repair cross grain tension specimen.

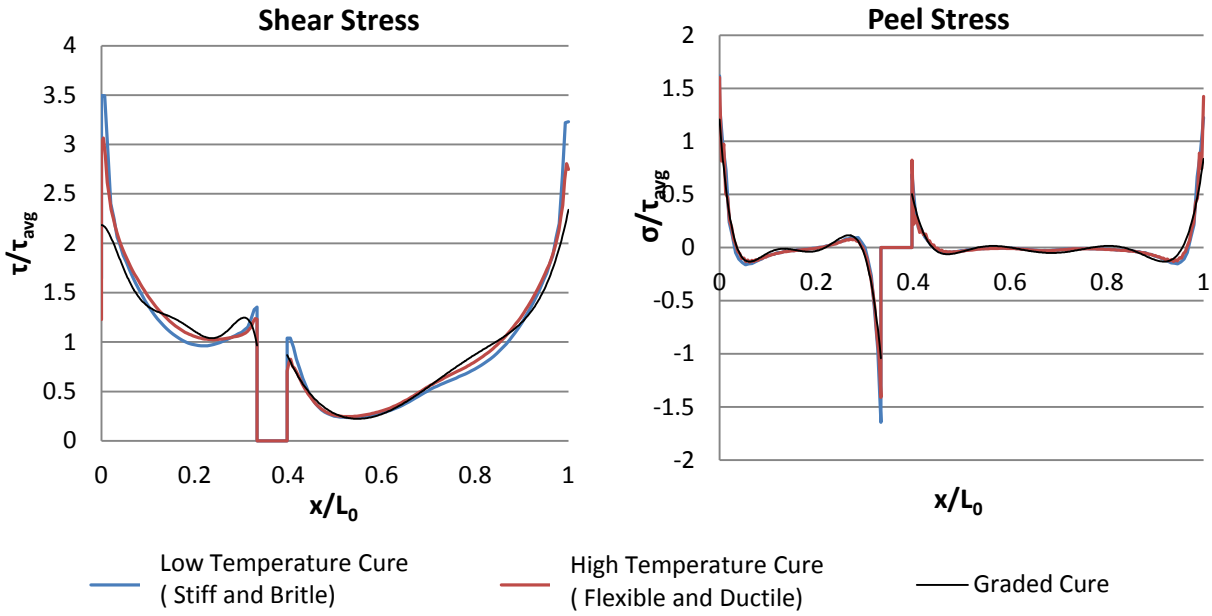

Figure 57: Shear and peel stress distribution in the 60 mm repair cross grain tension specimen.

Figure 56 and Figure 57 show that the maximum stress (both peel and shear) occur at the ends of the overlap. As in the compression specimens, the magnitudes of the peaks get higher with increasing lengths of the patches. The stress concentration factors are also higher for the adhesive cured at low temperature. The graded cure was able to create the most uniform stress distribution.

4.7 Strength Results

4.7.1 Undamaged Beam

Two fracture mechanisms were observed in the undamaged beam: pure tension (Figure 58-a) and cross grain tension (Figure 58-b). The cracks that were initiated by pure tension started, started to propagate in the RL plane. Only the specimens whose fibres were not exactly aligned failed by cross grain tension. All the others failed by simple tension bellow one of the loading cylinders.

These fracture mechanisms have also been observed by Campilho *et al.* (43).

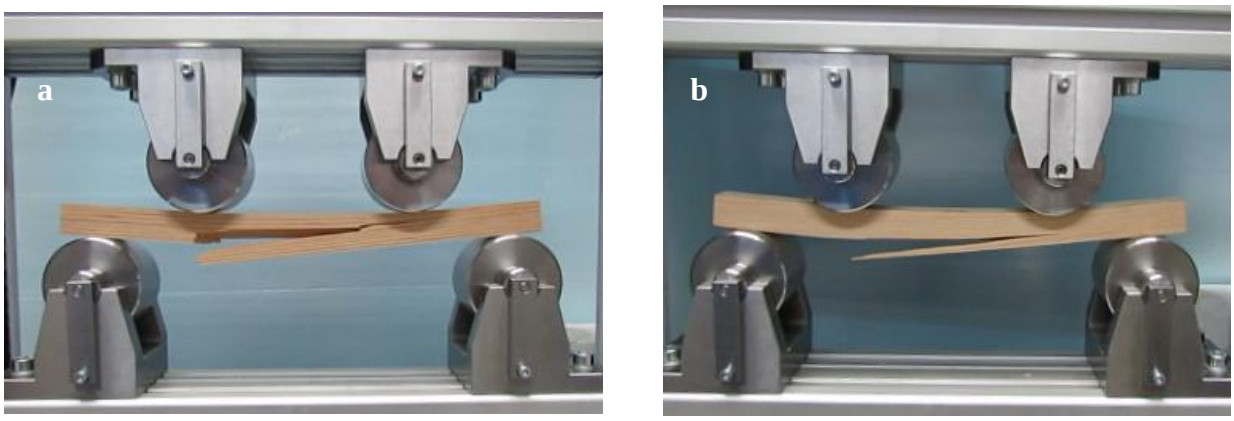

Figure 58: Failure mechanisms observed in the undamaged beam:

a- Simple tension
b- Cross grain tension

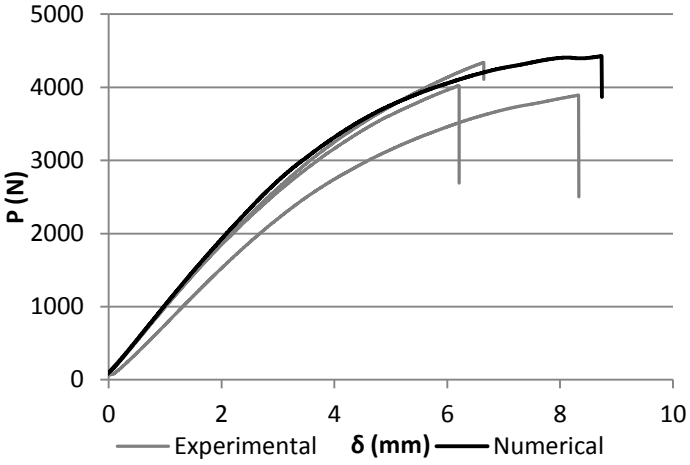

Figure 59: Experimental and numerical P-δ curves of the undamaged beam.

Figure 59 shows the experimental and numerical *P-δ* curves of the specimens. Failure occurred when P reached about 4171 N. The numerical simulation was able to accurately predict the strength of the beam.

As in the numerical model the grain is perfectly aligned, the numerical failure, like the experimental failure, occurred by simple tension under a loading cylinder.

4.7.2 Compression Damage Specimens

The unrepaired compression failure specimens failed in the wood mostly in the symmetry plane by pure tension (Figure 60-a). The specimens that exhibited a slight cross graining failed by cross grain tension (Figure 60-b).

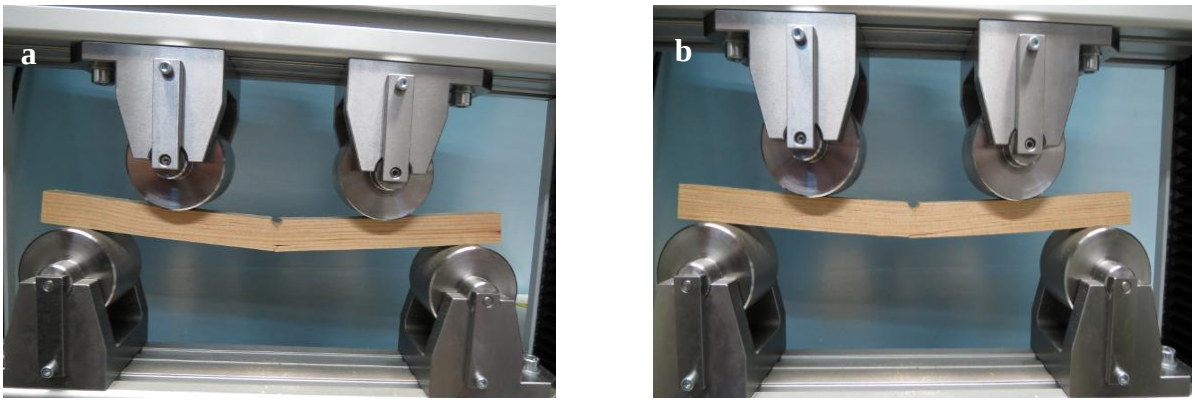

Figure 60: Failure mechanisms observed in the unrepaired compression damage specimens:

a- Simple tension
b- Cross grain tension

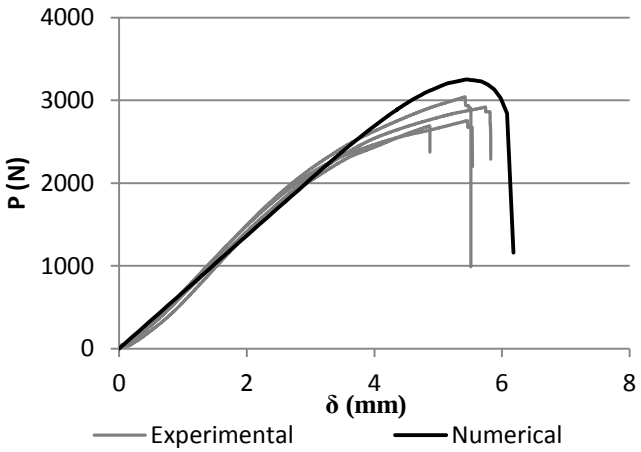

Figure 61: Experimental and numerical P-δ curves of the unrepaired compression specimen.

Figure 61: show the experimental and numerical P-δ curves of the unrepaired compression specimens. The average strength of the beams was about 2852 N.

The failure mechanisms reported for both the 20 mm repair and for the 30 mm repair were similar. Fracture occurred away from the repaired region, either by simple tension or, in the beams that exhibited slight cross graining, by cross grain tension (Figure 62). The failure of the 20 mm patch specimens that failed by simple tension initiated in the symmetry axel of the beam, while the 30 mm patch's started under one of the loading cylinders.

As failure occurred away from the repaired area, no conclusions could be made about the effectiveness of the different kinds of cure in the performance of the beams.

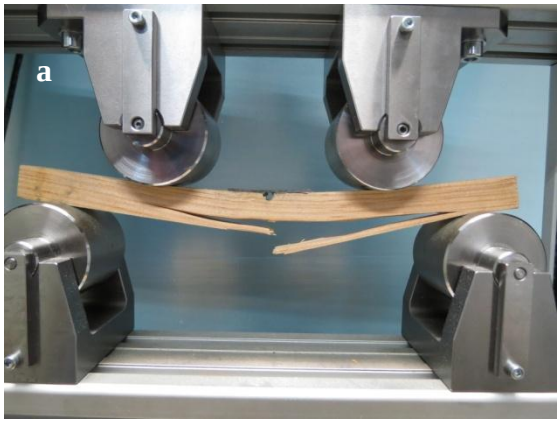

Figure 62: Failure mechanisms observed in the repaired compression damage specimens:

a- Simple tension (symmetry plane)
b- Simple tension (below the loading cylinder)
c- Cross grain tension

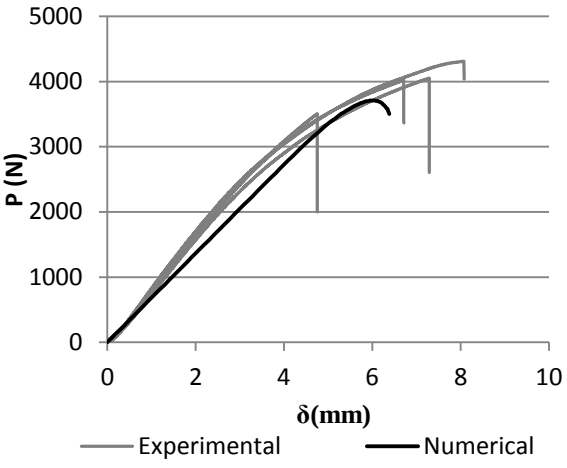

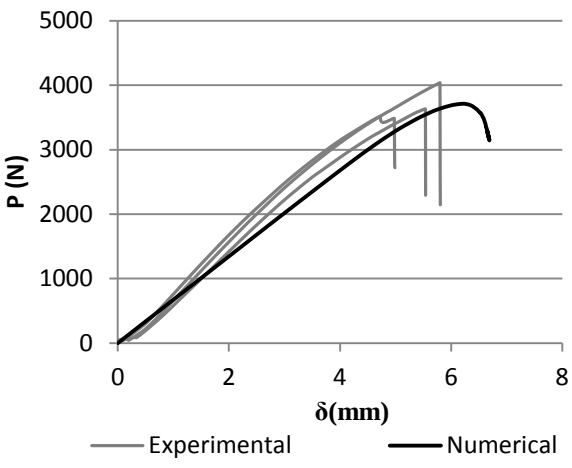

Figure 63: Experimental and numerical P-δ curves of the 20 mm repair compression specimens. Adhesive cured at 23°C (left) and at 100°C (right).

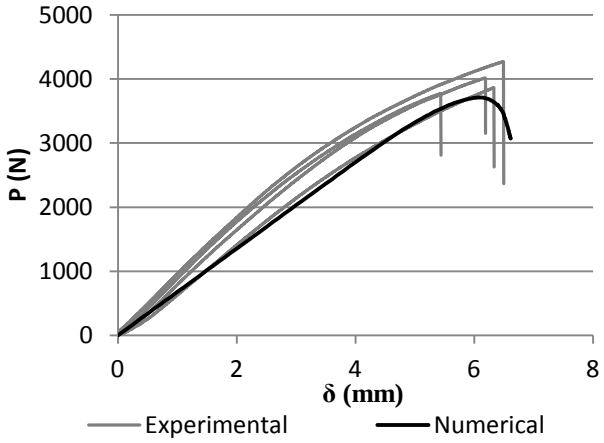

Figure 64: Experimental and numerical P-δ curves of the 20 mm repair compression specimen. Graded adhesive.

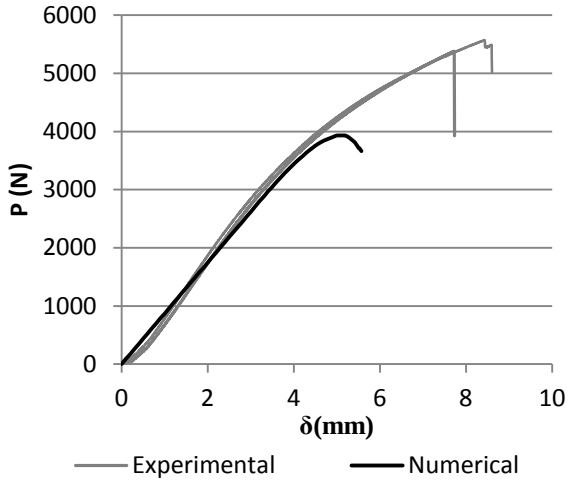

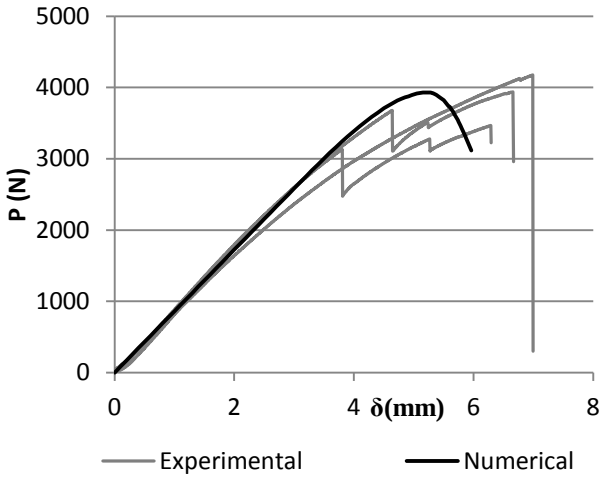

Figure 65: Experimental and numerical P-δ curves of the 30 mm repair compression damage specimens. Adhesive cured at 23^{o}C (left) and 100^{o}C (right).

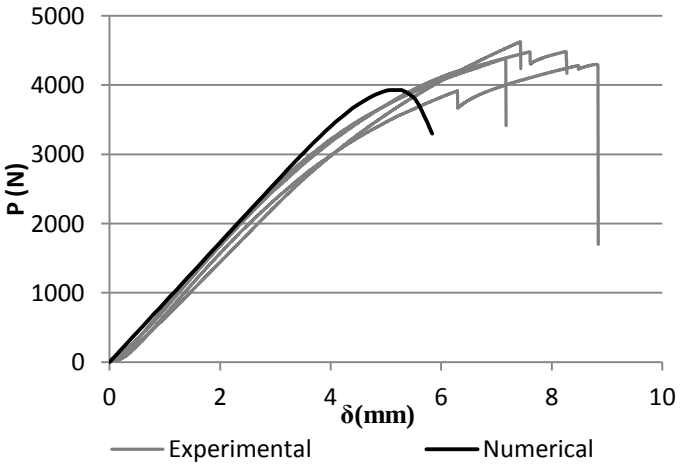

Figure 66: Experimental and numerical P-δ curves of the 30 mm repair compression damage specimens. Graded adhesive.

In the 20 mm and 30 mm compression failure specimens, failure occurred in the wood. The strength of the 20 mm compression failure specimens was lower than the strength of the 30 mm compression failure specimens because fracture occurred in the symmetry axel of the beam, influenced by the damaged area.

The FEM failure also shows the fracture occurring in the wood beam by simple tension in the symmetry axel of the beam for the 20 mm repair and below the loading cylinder for the 30 mm repair.

The beams repaired with the adhesive cured at 100^{o}C are slightly more compliant, as the adhesive cured at this temperature is more flexible.

The numerical results regarding the 23^{o}C and the graded cure 30 mm patch repairs did not match exactly the experimental results. As all other simulations were reasonably accurate, this is probably due to the natural variability of wood mechanical properties.

4.7.3 Cross Grain Tension Specimens

The damage in the unrepaired cross grain tension specimens initiated in the RL plane (Figure 67), on path 1 (Figure 69). Despite the drop in the stiffness of the beam, P continued to rise until a crack appeared on path 2 (Figure 69), leading to a drop in P. This is visible in the P-δ curves (Figure 68).

Figure 67: Failure mechanism of an unrepaired cross grain tension specimen

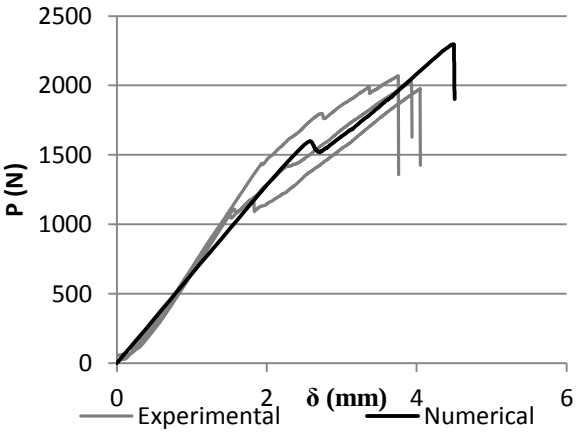

Figure 68: Experimental and numerical P-δ curves of the unrepaired cross grain tension specimens.

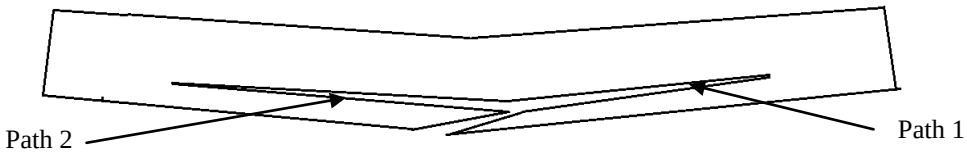

Figure 69: Schematic representation of paths 1 and 2.

Numerical failure also occurred first on path 1, with the consequent loss of stiffness, and then on path 2.

Failure in the repaired beams (for both the 40mm patch and the 60 mm patch specimens) occurred suddenly. Cracks appeared instantly, at the same time, in the adhesive-wood interface and paths 1 and 2 (Figure 70).

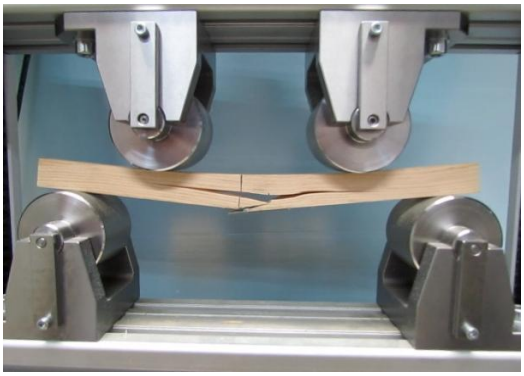

Figure 70: Failure mechanism of a repaired cross grain tension specimen.

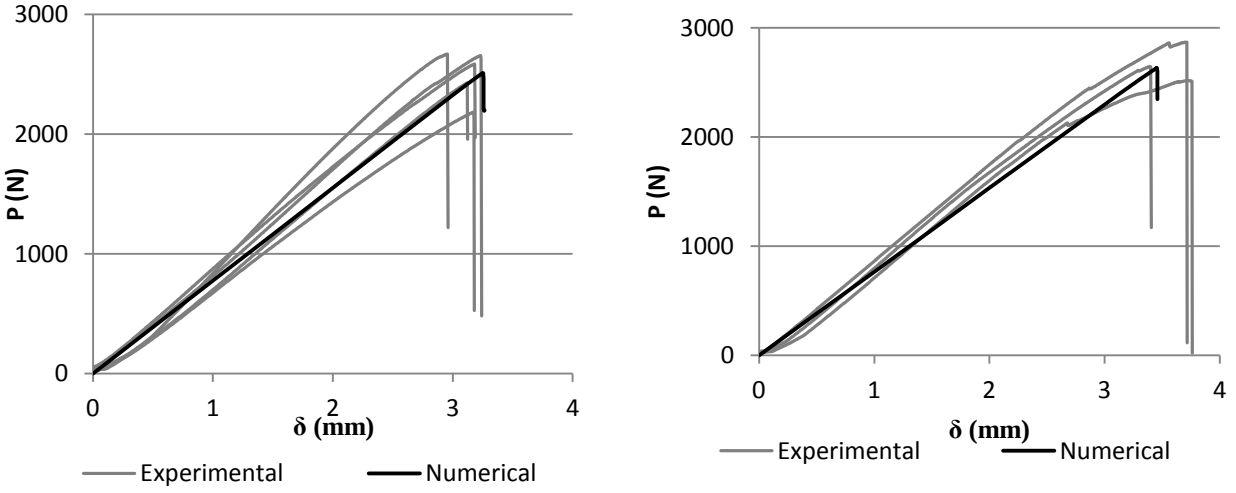

Figure 71: Experimental and numerical P-δ curves of the 40 mm repair cross grain tension specimens. Adhesive cured at 23°C (left) and at 100°C (right).

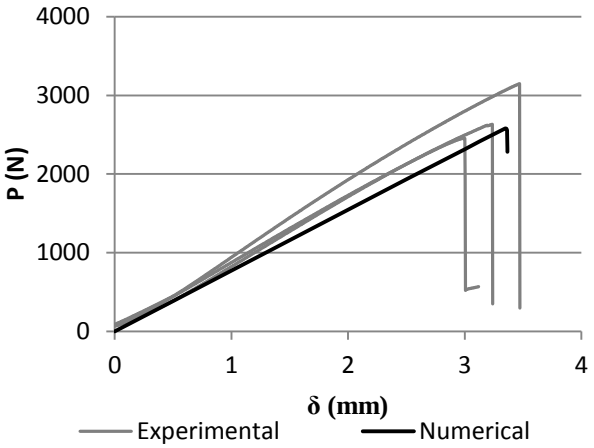

Figure 72: Experimental and numerical P-δ curves of the 40 mm repair cross grain tension specimens. Graded adhesive.

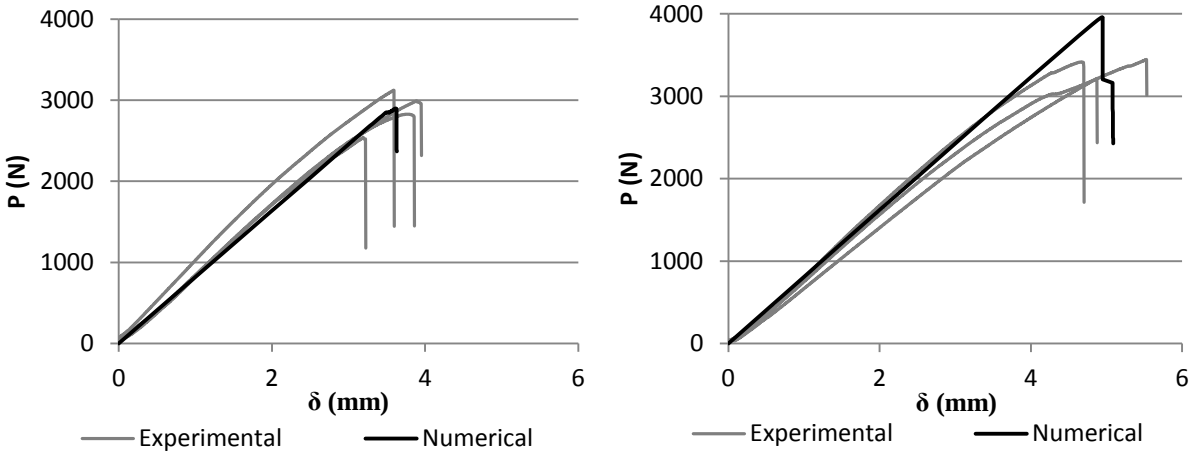

Figure 73: Experimental and numerical P-δ curves of the 60 mm repair cross grain tension specimens. Adhesive cured at 23°C (left) and at 100°C (right).

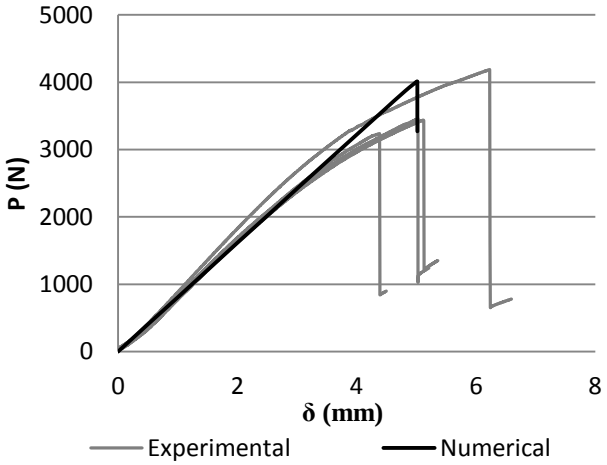

Figure 74: Experimental and numerical P-δ curves of the 60 mm repair cross grain tension specimens. Graded cure.

Figures 71-74 show that the strength of the beam increases with the patch length (L_0). The beams repaired with the ductile adhesive were stronger than the beams repaired with the brittle adhesive. The strongest beams were those repaired with the graded adhesive.

Numerical failure started in the adhesive-wood interface. At this stage, a drop in P occurred. The crack propagated first to path 1 and then to path 2.

4.8 Discussion of the Results

Table 8 summarizes the results of the 4PB tests

Table 8: Average strength of the specimens.

Specimen	L_0	T_{cure}	P_{max} [N]
Compression Specimen	20 mm	23°C	3973.5±467.4
		100°C	3734.0±303.1
		Graded	3981.7±289.4
	30 mm	23°C	4926.6±647.0
		100°C	3859.7±392.8
		Graded	4447.3±149.3
	Unrepaired		2852.4±190.,7
Cross Grain Tension Specimen	40 mm	23°C	2504,7±320,8
		100°C	2677.1±191.9
		Graded	2745.1±403.3
	60 mm	23°C	2872.1±329.6
		100°C	3391.4±175.6
		Graded	3579.8±608.7
	Unrepaired		2485.3±174.2
Undamaged Beam	-		4171.3±277.2

Figure 75 and Figure 76 show the improvement in the strength of the specimen versus an unrepaired beam and an undamaged beam respectively.

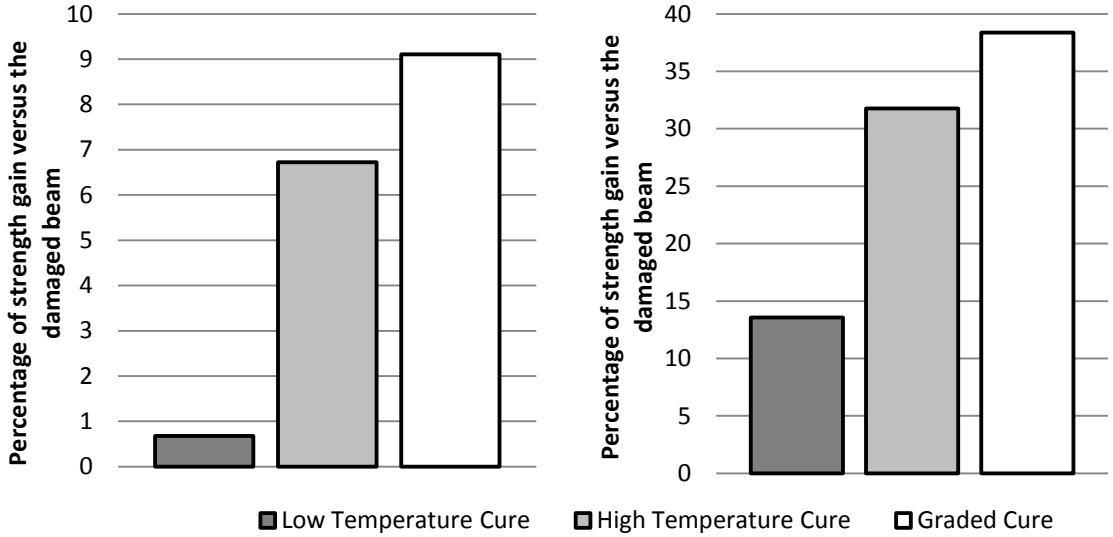

Figure 75: Strength gain of the cross grain tension specimens versus the unrepaired beam. The 40 mm repair (left) and the 60 mm repair (right).

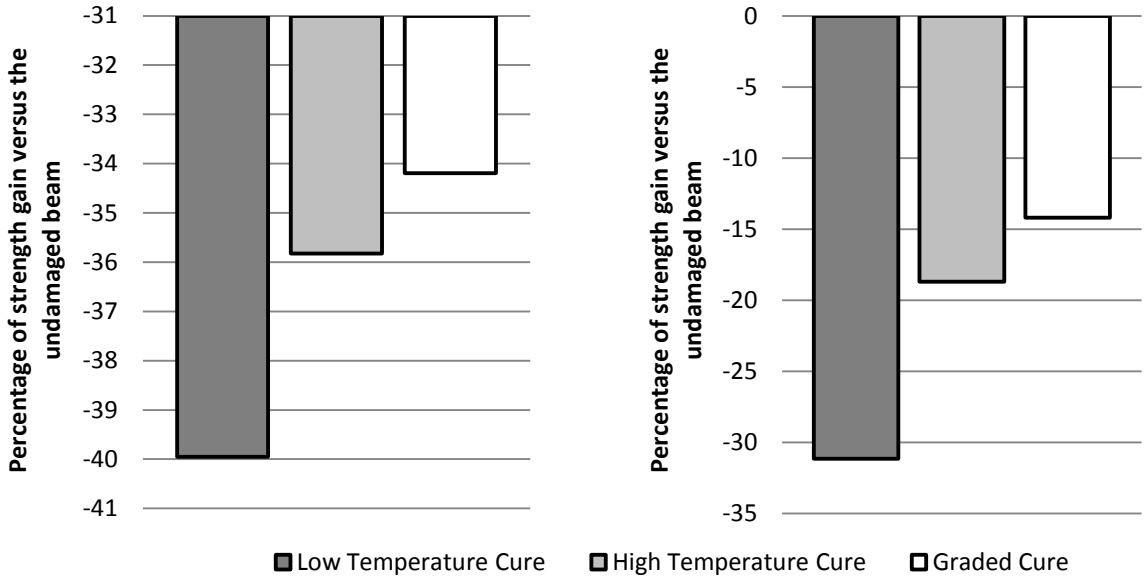

Figure 76: Strength gain of the cross grain tension specimens versus the undamaged beam. The 40 mm repair (left) and the 60 mm repair (right).

Figure 75 shows that the adhesive cured at high temperature (flexible behaviour) was more efficient in repairing wood beams damaged by cross grain tension than the adhesive cured at low temperature (brittle behaviour). The specimens repaired with a graded bondline showed the greatest strength and are the best choice when repairing wood structures. However, as

failure occurred in the repaired region, these patches were not able to restore the full strength of the beam, as can be seen in Figure 76. In order to fully repair the cross grain tension wood beams, longer patches should be used.

The great advantage of the graded joint is that the adhesive is ductile where there is great stress concentration and resistant where the stress concentration factor is low, however, as fracture occurred in the wood-adhesive interface, the adhesive was not allowed to develop its full ductility or strength. The improvement on the strength of the beams was due to the more uniform stress distribution, obtained with this kind of bondline.

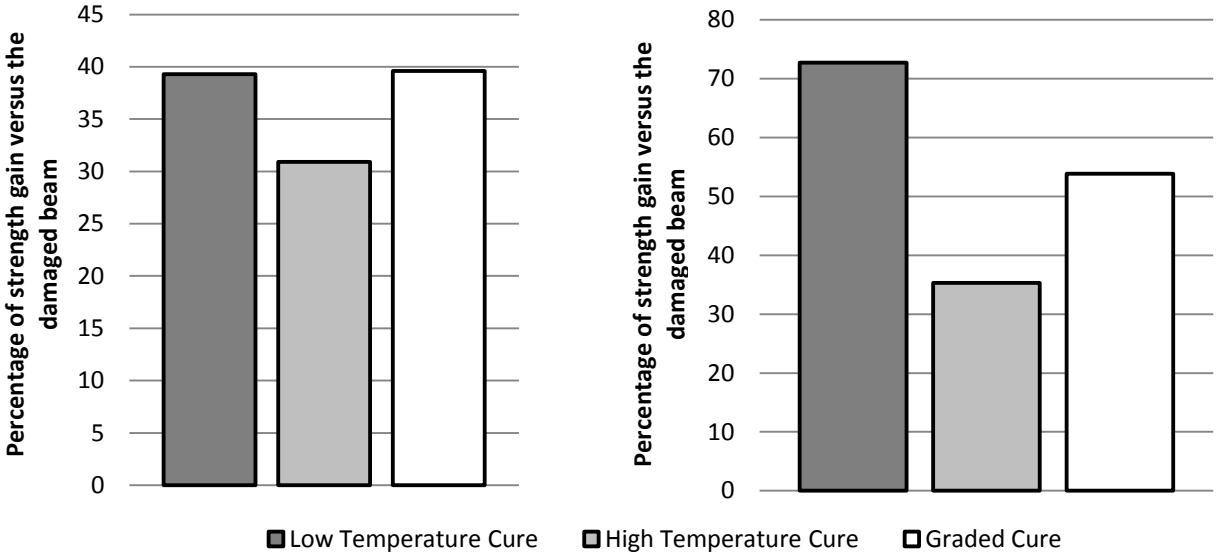

Figure 77: Strength gain of the compression specimens versus the unrepaired beam. The 20 mm repair (left) and the 30 mm repair (right).

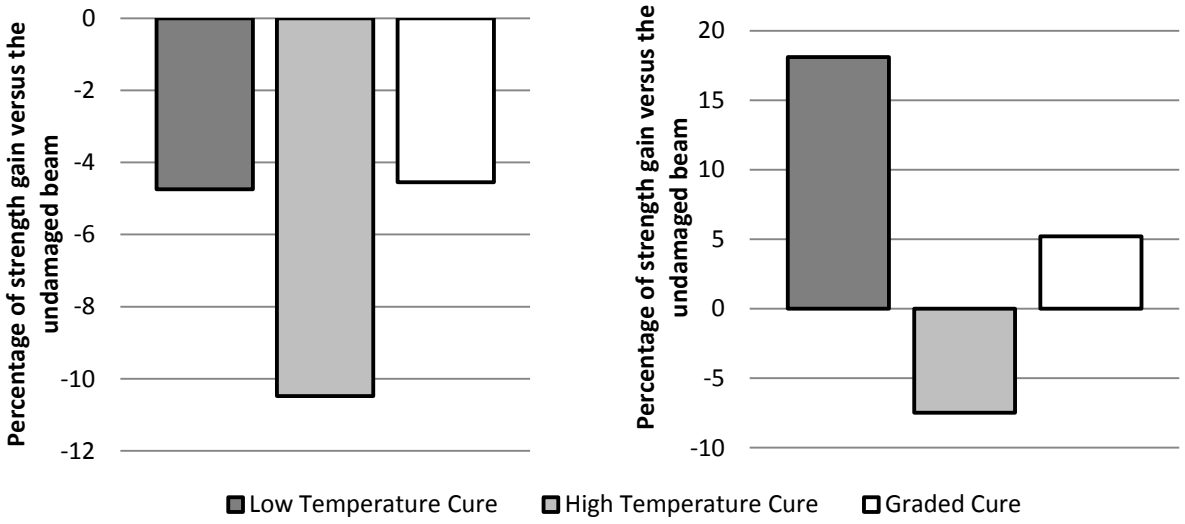

Figure 78: Strength gain of the compression specimens versus the undamaged beam. The 20 mm repair (left) and the 30 mm repair (right).

Finite element analyses show that there is no great difference between the kind of adhesive cure in the compression specimens. However, experiments have shown distinct values for all kinds of cure. As fracture occurred always in the wood, this might be due to the high dispersion of results expected to happen on wood specimens.

In the compression specimens, as fracture occurred always away from the repaired area, the failure of the specimens is conditioned by the existence of defects in the wood. As wood is a biological product, these defects have a wide dispersion. Some beams have many defects, others have very few defects. This reflects on the dispersion of results. In cross grain tension specimens, however, as fracture occurred always in the repaired area, the fracture is conditioned by a single defect that is almost equal for every specimen. This might be the reason why the dispersion of results is wider in the compression specimens than in the cross grain tension specimens.

5 Conclusions and Future Work

This study focused on the patch repair of wood structures with a functionally graded bondline. Two common types of defects of wood beams under bending loadings, cross grain tension and compression failure, were analysed. CFRP patches were bonded to the damaged area using the Locktite® Hysol 3422 adhesive. The effect of the cure cycle of the adhesive in the effectiveness of the repair was assessed. Three different cure cycles were studied: a low temperature cure (that makes the adhesive stiff and brittle), a high temperature cure (that makes the adhesive flexible and ductile) and a graded cure (that makes the adhesive ductile where there is greater stress concentration and strong where high strength is required).

These repairs were simulated with the FEM. CZM were used to simulate the crack initiation and propagation. In order to be able to simulate the fracture behaviour of the adhesive layer, DCB and ENF tests were performed and the toughness of the adhesive in modes I and II for different temperatures of cure was determined.

The results concerning the bending tests on the wood beams showed that graded joints can be used to improve the strength and reliability of repaired beams. The numerical simulations were able to predict the behaviour of the wood specimens, including the specimens repaired with a graded bondline.

The following future investigations are recommended:

- Determine the toughness of the adhesive for more temperatures of cure;
- Choose another configuration for the compression damage specimens to make sure that the specimens fail in the repaired region;
- Develop a FEM formulation that is able to simulate the behaviour of a material with graded properties. This would allow the user to simulate the behaviour of a graded adhesive without the need to divide the bondline in several partitions;
- It would be interesting to know with more detail the distribution of temperature during the graded cure of the adhesive. In order to do this, the FEM could be used;
- Repeat the tests with other adhesives.

6 References

1. **Akbiyik, A.** Feasibility Investigation into Shear Repair of Timber Bridge Stringers. 2005.

2. **Ebeling, D. W.** Repair and rehabilitation of heavy timber trusses. 1990, Vol. 4, pp. 242-258.

3. **J. Custódio, J. Broughton, H. Cruz.** A review of factors influencing the durability of structural bonded timber joints. 2009, Vol. 29, pp. 173– 185.

4. **M.F. Humphreys, K. L. Francey.** An investigation into the rehabilitation of timber structures with fibre composite materials', Developments in Mechanics of Structures and Materials. 2004.

5. **P. Alam, M. P. Ansell, D. Smedley.** Mechanical repair of timber beams fractured in flexure using bonded-in reinforcements. 2009, Vol. 40, pp. 95–106.

6. **R. D. S. G. Campilho, M. F. S. F. de Moura., D. A. Ramantani, J. J. L. Morais, A. M. J. P. Barreto and J. J. M. S. Domingues.** Adhesively Bonded Repair Proposal for Wood Members Damaged by Horizontal Shear Using Carbon-Epoxy Patches. 2010, Vol. 86, pp. 649–670.

7. **R. D. S. G. Campilho, M. F. S. F. de Moura, A. M. J. P. Barreto, J. J. L. Morais, J. J. M. S. Domingues.** Fracture behaviour of damaged wood beams repaired with an adhesively-bonded composite patch. 2009, Vol. 40, pp. 852–859.

8. **R. D. S. G. Campilho, M. F. S. F. de Moura, A. M. J. P. Barreto, J. J. M. S. Domingues, J. J. L. Morais.** Experimental and numerical evaluation of composite repairs on wood beams damaged by cross-graining. 2010, Vol. 24, pp. 531–537.

9. **L. F.M. da Silva, A. Öchsner, R. D. Adams.** Handbook of Adhesion Technology. 2011, Vol. 1, p. 702.

10. **S. E. Stapleton, A. M. Waas, S. M. Arnold.** Functionally graded adhesives for composite joints. 2012, Vol. 35, pp. 36-49.

11. **R. J. C. Carbas, E. A. S. Marques, L. F. M. da Silva, A. M. Lopes.** Effect of cure temperature on the glass transition temperature and mechanical properties of epoxy adhesives. 2013.

12. **M. F. S. F. de Moura, R. D. S. G. Campilho., J. P. M. Gonçalves.** Crack equivalent concept applied to the fracture characterization of bonded joints under pure mode I loading. 2008, Vol. 68, pp. 2224–2230.

13. **M. F. S. F. de Moura, A. B. de Morais.** Equivalent crack based analyses of ENF and ELS tests. 2008, Vol. 75, pp. 2584-2596.

14. **A. Akbiyik, A. J. Lamanna, W. M. Hale.** Feasibility investigation of the shear repair of timber stringers with horizontal splits. 2007, Vol. 21, pp. 991–1000.

15. **A. G. Christy, T.J. Senden, P. D. Evans.** Automated measurement of checks at wood surfaces. 2005, Vol. 37, pp. 109–118.

16. **F. Lionetto, M. Frigione.** Mechanical and natural durability properties of wood treated with a novel organic preservative/consolidant product. 2009, Vol. 30, pp. 3303–3307.

17. **D. W. Radford, D. Van Goethem, R. M. Gutkowski, M. L. Peterson.** Composite repair of timber structures. 2008, Vol. 16, pp. 417–425.

18. **L. F. M. da Silva, R.D.Adams.** Techniques to reduce the peel stresses in adhesive joints with composites. 2007, Vol. 27, pp. 227-235.

19. **Volkersen, O.** *Luftfahrtforschung.* 1938. pp. 15-41.

20. **M. Golland, E. Reissner.** *Journal of Applied Mechanics.* 1944, pp. A17-27.

21. **L. F. M. da Silva, T. N. S. S. Rodrigues, M. A. V. Figueiredo, M. F. S. F. de Moura, J. A. G. Chousal.** Effect of Adhesive Type and Thickness on the Lap Shear Strength. 2006, Vol. 82, pp. 1091–1115.

22. **Adams, Peppiatt.** *J Strain Anal.* 1974, Vol. 9, p. 185.

23. **Crocombe, A. D.** *Int j adhes Adhes.* 1989, Vol. 9, p. 145.

24. **L. F. M. da Silva, T. N. S. S. Rodrigues, M. A. V. Figueiredo, M. F. S. F. de Moura, J. A, G. Chousal.** *Journal of Adhesion.* 2006, Vol. 82, pp. 1091-115.

25. **R. D. S. G. Campilho, M. F. S. F. de Moura, J .J. M. S. Domingues.** Modelling single and double-lap repairs on composite materials. 2005, Vol. 65, pp. 1948–1958.

26. **E. A. S. Marques, L. F. M. da Silva.** Joint Strength Optimization of Adhesively Bonded Patches. 2008, Vol. 84, pp. 915–934.

27. **T. P. Lang, P.K. Mallick.** Effect of spew geometry on stresses in single lap adhesive joints. 1998, Vol. 18, pp. 167-177.

28. **R. D. Adams, J. A. Harris.** *Int J Adhes Adhes.* 1987, pp. 7-69.

29. **X. Zhao, R. D. Adams, L. F. M. da Silva.** Single Lap Joints with Rounded Adherend Corners: Stress and Strain Analysis. *Journal of Adhesion Science and Technology.* 2011, Vol. 25, pp. 819-836.

30. **L. F. M. da Silva, M. J. C. Q. Lopes.** Joint strength optimization by the mixed-adhesive technique. 2009, Vol. 29, pp. 509-514.

31. **M. Kemal Apalak, R. Gunes.** Elastic flexural behaviour of an adhesively bonded single lap joint with functionally graded adherends. 2007, Vol. 28, pp. 1597-1617.

32. **M. K. Apalak, R. Gunes.** Investigation of elastic stresses in an adhesively bonded single lap joint with functionally graded adherends in tension. 2005, Vol. 70, pp. 444-467.

33. **V. K. Ganesh, T. S. Choo.** Modulus Graded Composite Adherends for Single-Lap Bonded Joints. *GoodForm Composite Technologies.* 2002, Vol. 36, p. 1757.

34. **R. J. C. Carbas, L. F. M. da Silva, G. W. Critchlow.** Functionally Graded Joints by Induction Heating, patent submited.

35. —. Adhesively Bonded Functionally Graded Joints by Induction Heating. *Int. J. Adhe. Adhe. to be submited.*

36. **L. F. M. da Silva, R. D. S. G. Campilho.** Advances in Numerical Modelling of Adhesive Joints. *Springer Briefs in Computational Mechanics.* 2012.

37. **C. D. M. Liljedahi, A. D. Crocombe, M. A. Wahab, I. A. Ashcroft.** Damage modelling of adhesively bonded joints. *Int. J. Fract.* 2006, Vol. 141, pp. 147-161.

38. **R. J. C. Carbas, L. F. M. da Silva, E. A. S. Marques, A. M. Lopes.** Effect of Post-Cure on the Glass Transition Temperature and Mechanical Properties of Epoxy Adhesives. 2013.

39. **M. F. S. F. De Moura, J. P. M. Gonçalves, J. A. G. Chousal, R. D. S. G. Campilho.** Cohesive and continuum mixed-mode damage models applied to the simulation of the mechanical behaviour of bonded joints. 2008, Vol. 28, pp. 419– 426.

40. **M. F. S. F. de Moura, M. A. L. Silva, A. B. de Morais, J. J. L. Morais.** Equivalent crack based mode II fracture characterization of wood. 2006, Vol. 73, pp. 978-993.

41. **J. L. Pereira, J. Xavier, J. Morais.** Estudo por elementos finitos dum novo método para a determinação das propriedades mecânicas da madeira de Pinus Pinaster ait. nas direcções perpendiculares ao grão.

42. **M. F. S. F. de Moura, J. J. L. Morais, N. Dourado.** A new data reduction scheme for mode I wood fracture characterization using the double cantilever beam test. 2008, Vol. 75, pp. 3852–3865.

43. **Campilho, R. D. S. G.** *Repair of Composite and Wood Structures.* Department of Mechanical Engineering and Industrial Management, Faculty of Engineering of Porto University. Porto, Portugal : s.n., 2008.

44. **E. F. Karachalios, R. D. Adams, L. F. M. da Silva.** *Int J. Adhes. Adhes.* 2013, Vol. 43, pp. 81-95.